

AGN AND STARBURST RADIO EMISSION FROM OPTICALLY SELECTED QSOs

J. J. CONDON¹, K. I. KELLERMANN¹, AND AMY E. KIMBALL¹
National Radio Astronomy Observatory, 520 Edgemont Road, Charlottesville, VA 22903, USA

ŽELJKO IVEZIĆ
Department of Astronomy, University of Washington, Box 351580, Seattle, WA 98195, USA

R. A. PERLEY¹
National Radio Astronomy Observatory, Socorro, NM 87801, USA
Draft version August 27, 2018

ABSTRACT

We used the 1.4 GHz NVSS to study radio sources in two color-selected QSO samples: a volume-limited sample of 1313 QSOs defined by $M_i < -23$ in the redshift range $0.2 < z < 0.45$ and a magnitude-limited sample of 2471 QSOs with $m_r \leq 18.5$ and $1.8 < z < 2.5$. About 10% were detected above the 2.4 mJy NVSS catalog limit and are powered primarily by AGNs. The space density of the low-redshift QSOs evolves as $\rho \propto (1+z)^6$. In both redshift ranges the flux-density distributions and luminosity functions of QSOs stronger than 2.4 mJy are power laws, with no features to suggest more than one kind of radio source. Extrapolating the power laws to lower luminosities predicts the remaining QSOs should be extremely radio quiet, but they are not. Most were detected statistically on the NVSS images with median peak flux densities S_p (mJy beam⁻¹) ≈ 0.3 and 0.05 in the low- and high-redshift samples, corresponding to spectral luminosities $\log[L_{1.4\text{ GHz}}(\text{W Hz}^{-1})] \approx 22.7$ and 24.1, respectively. We suggest that the faint radio sources are powered by star formation at rates $\dot{M} \sim 20M_\odot \text{ yr}^{-1}$ in the moderate luminosity (median $\langle M_i \rangle \approx -23.4$) low-redshift QSOs and $\dot{M} \sim 500M_\odot \text{ yr}^{-1}$ in the very luminous ($\langle M_i \rangle \approx -27.5$) high-redshift QSOs. Such luminous starbursts [$\langle \log(L_{\text{IR}}/L_\odot) \rangle \sim 11.2$ and 12.6, respectively] are consistent with “quasar mode” accretion in which cold gas flows fuel both AGN and starburst.

Subject headings: galaxies: active—galaxies: starburst—quasars: general—radio continuum: galaxies

1. INTRODUCTION

The radio emission from quasi-stellar objects (QSOs) has puzzled astronomers for nearly 50 years. The first QSOs to be recognized contain very strong radio sources similar to those powered by the active galactic nuclei (AGNs) of the most luminous radio galaxies, but $\sim 90\%$ of bright optically selected QSOs are fainter than 1 mJy at 1.4 GHz. Also, the flux-density distribution of radio-loud QSOs is quite different from that of radio galaxies, and might even be bimodal. These differences led to longstanding debates about whether QSOs experience the same cosmological evolution as radio galaxies and whether there are two distinct types of radio sources in QSOs. In this paper, we use direct detections of radio sources stronger than 2.4 mJy and statistical detections of fainter sources in two large samples of QSOs to argue that (1) radio-loud QSOs are similar to powerful radio galaxies and do evolve, despite their differing flux-density distributions, and (2) radio-quiet QSOs really are different from radio-loud QSOs because most of their radio emission is powered by starbursts instead of AGNs. Since the problem of radio emission from QSOs has such a long and complicated history, we begin with a short review to

set the stage and define common terms.

1.1. Quasars, QSGs, and QSOs

Hazard et al. (1963), Schmidt (1963), and Matthews & Sandage (1963) found the first quasi-stellar radio sources (quasars or QSSs) by optically identifying redshifted “stars” with radio sources whose luminosities are “not markedly different from other known strong radio sources like Cygnus A or 3C 295” (Greenstein & Matthews 1963) in elliptical galaxies. The first optically selected quasi-stellar galaxies (QSGs) found by Sandage (1965) “resemble the quasi-stellar radio sources in many optical properties, but they are radio quiet” in the sense that only about one QSG per thousand brighter than $m_{\text{pg}} = 19$ appeared in the relatively insensitive all-sky radio catalogs of the time ($S > 9 \text{ Jy}$ at 178 MHz). All of the first quasars and QSGs appear starlike because their AGNs are far more luminous than their inferred host galaxies, assuming their redshifts are cosmological. The deliberately vague name “quasi-stellar object” (QSO) still used today for both quasars and QSGs was introduced by Hoyle & Burbidge (1966) because they doubted the redshifts of the QSGs were cosmological and so “at this stage we do not think enough is known about their nature for a definitive name to be chosen.”

Although QSGs were called “a major new constituent of the universe” by Sandage (1965), they are not a dis-

jcondon@nrao.edu

¹The National Radio Astronomy Observatory is a facility of the National Science Foundation operated under cooperative agreement by Associated Universities, Inc.

tinct constituent, only the luminous tail of a continuous distribution that includes Seyfert galaxies whose AGNs do not overwhelm their starlight. Schmidt & Green (1983) formally distinguished them from Seyfert galaxies by requiring QSOs contain AGNs brighter than $M_B = -23$, the absolute magnitude of the brightest galaxies of stars calculated using $H_0 = 50 \text{ km s}^{-1} \text{ Mpc}^{-1}$ and $q_0 = 0.1$. In the modern flat Λ CDM cosmology with $H_0 = 71 \text{ km s}^{-1} \text{ Mpc}^{-1}$ and $\Omega_m = 0.27$, the brightest galaxies have $M_B \approx -22.2$, so the spirit of the Schmidt & Green (1983) criterion (QSOs contain AGNs brighter than any host galaxy of stars) would change the QSO cutoff to $M_B \approx -22.2$. However, like most authors, we follow the letter ($M_B = -23$) of the Schmidt & Green (1983) criterion. Thus our least-luminous QSOs are actually about twice as luminous as the brightest galaxies. The value of this cutoff matters because such luminous QSOs are rarely found in spiral galaxies (Dunlop et al. 2003).

1.2. QSOs Versus Radio Galaxies

The cumulative radio flux-density distribution of the strongest radio galaxies rises slightly faster than the Euclidean rate

$$N(> S) = \int_S^\infty n(s) ds \propto S^{-1.5}, \quad (1)$$

where $N(> S)$ is the cumulative number of sources per steradian stronger than S and $n(S)dS$ is the differential number per steradian with flux densities S to $S + dS$. If the same were true of bright QSOs and there is one radio-loud QSO stronger than 10 Jy among 1000 optically selected QSOs, one might hope to find 30 radio sources stronger than 1 Jy and hundreds above 0.1 Jy. From this perspective, the first directed searches for radio emission from optically selected QSOs were surprisingly unsuccessful (Kellermann & Pauliny-Toth 1966). Radio sources were detected in only about 10% of bright QSOs even after decades of increasingly sensitive searches (Katgert et al. 1973; Strittmatter et al. 1980; Miller et al. 1990) for sources as faint as 0.01 Jy at $\nu = 1.4 \text{ GHz}$, or $\log[L_\nu(\text{W Hz}^{-1})] \approx 24$ at $z \approx 0.2$. These low detection rates imply that the flux-density distribution of optically selected QSOs rises much more slowly and may even be bimodal. They might also indicate that QSOs and radio galaxies do not experience the same amount of cosmological evolution (Miller et al. 1990).

1.3. Are There Two Distinct Populations of QSOs?

Strittmatter et al. (1980) were the first to report a bimodal QSO flux-density distribution, with an observed peak near $S = 1 \text{ Jy}$ and an inferred peak at $S < 10 \text{ mJy}$, albeit in a very small sample. Miller et al. (1990) noted a bimodal luminosity distribution implied by the bimodal flux-density distribution of their larger sample of QSOs in the redshift range $1.8 < z < 2.5$. They found nine radio sources with $\nu = 5 \text{ GHz}$ spectral luminosities $\log[L_\nu(\text{W Hz}^{-1})] > 26$, 96 upper limits below $\log[L_\nu(\text{W Hz}^{-1})] \approx 25$, and nothing in between. The term ‘‘bimodal’’ is perhaps too strong: a bimodal distribution has two peaks. Neither Strittmatter et al. (1980) or Miller et al. (1990) actually detected the low-luminosity peak; its existence was only inferred from the

large number of nondetections whose radio flux densities or luminosities would have to be spread smoothly over many orders of magnitude to not yield a second peak. For a recent analysis of bimodality in light of modern optical and radio data, see Baloković et al. (2012).

A bimodal flux-density or luminosity distribution suggests there may be two distinct populations of radio sources in QSOs. For example, Miller et al. (1990) associated their high-luminosity peak with AGNs in elliptical galaxies similar to the hosts of radio galaxies and the inferred low-luminosity peak with weaker AGNs in spiral galaxies. However, *any* nonuniformity or feature in these distributions is sufficient to suggest two distinct populations. Bimodality is sufficient but not necessary, so we suggest that debates about whether a clearly visible feature in a distribution makes it truly bimodal are not relevant to the fundamental question ‘‘Are there two distinct populations of QSOs?’’

1.4. Further Complications

Three factors have complicated investigations of QSO radio luminosity functions:

(1) The radio/optical luminosity ratio of QSOs might be a better measure of radio loudness than absolute radio luminosity alone. Schmidt (1970) proposed that the radio luminosity function ‘‘depends on the optical luminosity in such a manner that the ratio has a universal distribution function’’ of the form

$$\Phi(F_o, F_r) = \Phi(F_o)\Psi(F_r/F_o). \quad (2)$$

Equation 2 implies a linear correlation between radio and optical luminosities, so the radio/optical ratio

$$R \equiv F_r/F_o \quad (3)$$

may be a better indicator of radio activity. Peacock et al. (1986) countered that almost no radio-loud QSOs are optically fainter than $M_B = -24$ (for $H_0 = 50 \text{ km s Mpc}^{-1}$ and $q_0 = 0.1$, equivalent to $M_B > -23.2$ for today’s Λ CDM model), so that an apparent correlation in the data may only reflect differences between two populations of QSO host galaxies, optically luminous ellipticals and optically fainter spirals. Using FIRST (Becker, White, & Helfand 1995) direct and statistical detections of QSOs in a very large sample, White et al. (2007) found a clear but nonlinear correlation of radio and optical luminosities $F_r \propto F_o^{0.85}$. However, Appendix C of Ivezić et al. (2002) argues that selection effects are responsible for such apparent correlations.

(2) Flux-density boosting in relativistic [$\gamma^2 \equiv (1 - v^2/c^2)^{-1} \gg 1$] radio jets may significantly broaden both the radio flux-density and the R distributions of QSOs, whose optical emission does not appear to be strongly beamed (Scheuer & Readhead 1979). Thus radio jets in optically selected QSOs should be randomly oriented relative to our line-of-sight, but only the small fraction $\approx \gamma^{-2}$ of QSOs whose jets are aligned near our line-of-sight become radio-loud quasars. The geometry of relativistic beaming tends to flatten the differential count of QSO radio sources from $n(S) \propto S^{-5/2}$ towards $n(S) \propto S^{-4/3}$ [or $N(> S) \propto S^{-1/3}$] for intrinsically steep-spectrum ($\alpha \equiv d \ln S / d \ln \nu \sim -1$) sources.

(3) Like the optical emission from a QSO, the radio emission is the sum of two known components,

one powered by the AGN and the other by the host galaxy of stars. Massive stars born within the past $\sim 10^8$ years and relativistic electrons accelerated by their supernova remnants power the radio emission from the host galaxy, so a “red and dead” elliptical galaxy with no recent star formation can be extremely radio-quiet (Walsh et al. 1989). A number of features can be used to distinguish between these two types of radio source. The most powerful nearby starburst is in the ultraluminous infrared galaxy Arp 220, whose spectral luminosity is $\log[L_{1.4\text{ GHz}}(\text{W Hz}^{-1})] \approx 23.5$. Although the western nucleus of Arp 220 appears to contain an obscured AGN with X-ray luminosity $L_x \sim 10^{44} \text{ erg s}^{-1}$ (Rangwala et al. 2011), the compact radio component in the western nucleus accounts for less than 25% of the integrated 1.4 GHz radio flux density (Mundell, Ferruit, & Pedlar 2001), so the Arp 220 starburst luminosity is not less than $\log[L_{1.4\text{ GHz}}(\text{W Hz}^{-1})] \approx 23.4$. A starburst-powered radio source is roughly coextensive with the starburst and is not brighter than $T_b \sim 10^5 \text{ K}$ at 1.4 GHz, has the steep spectrum $\alpha \sim -0.7$ at centimeter wavelengths typical of optically thin synchrotron radiation, obeys the far-infrared (FIR)/radio correlation (Condon 1992), and is not strongly variable. In contrast, an AGN can produce a radio source several orders of magnitude more luminous than $\log[L_{1.4\text{ GHz}}(\text{W Hz}^{-1})] \sim 24$, its radio jets and lobes can extend far outside the host galaxy of stars, and its radio core can be small enough to vary significantly on time scales of years (Barvainis et al. 2005). The radio spectrum of an AGN can be nearly flat ($\alpha \sim 0$) over a wide frequency range, either from a synchrotron self-absorption “conspiracy” among compact components (Cotton et al. 1980) or from optically thin free-free radiation by a hot $T > 10^7$ AGN disk wind (Blundell & Kuncic 2007). However, Steenbrugge et al. (2011) found that “for 20 out of 22 PG quasars studied, free-free emission from a wind emanating from the accretion disc cannot mutually explain the observed radio and X-ray luminosity,” eliminating free-free emission as the cause of the radio-quiet peak in the luminosity distribution of QSOs.

Nearly all low-redshift ($z < 0.5$) radio galaxies seem to be “red and dead” ellipticals whose radio sources are powered primarily by their AGNs. By analogy, low-redshift QSOs whose radio sources are (1) more luminous than $\log[L_{1.4\text{ GHz}}(\text{W Hz}^{-1})] \sim 24$, (2) have lower FIR/radio flux-density ratios than starburst galaxies, (3) are either larger than $\sim 20 \text{ kpc}$ or very compact (Falcke et al. 1996; Blundell & Beasley 1998; Ulvestad et al. 2005), (4) are strongly variable (Barvainis et al. 2005) or (5) have flat radio spectra probably reside in elliptical galaxies. This analogy is supported by high-resolution *HST* images of nearby QSO host galaxies (Boyce et al. 1998; Dunlop et al. 2003). QSOs close to the original Schmidt & Green (1983) luminosity limit often obey the FIR/radio correlation, may contain starburst-dominated radio sources (e.g., Barvainis 1990; Sopp & Alexander 1991; Barthel 2006; de Vries et al. 2007), and may be in disc or merging galaxies (Boyce et al. 1998). In contrast, Dunlop et al. (2003) found that QSOs having nuclear luminosities $V < -23.5$ (assuming $H_0 = 50 \text{ km s}^{-1} \text{ Mpc}^{-1}$, or $V < -22.7$

in modern Λ CDM cosmology) are virtually all massive ellipticals with no large-scale star formation. Weak radio emission correlated with the strength of the 4000 Å break indicates that star formation is quite common in the host galaxies of low-luminosity AGNs (de Vries et al. 2007). We conclude that the radio properties of QSO samples are likely to depend on the absolute magnitude cutoff, and samples containing low-luminosity AGNs should not be used to infer the radio properties of true QSOs.

The 1.4 GHz flux density of an ultraluminous starburst galaxy like Arp 220 would be only $S \approx 0.4 \text{ mJy}$ at $z \approx 0.5$ and $S \approx 0.015 \text{ mJy}$ at $z \approx 2$, so exceptionally sensitive observations are needed to characterize the starburst radio emission from individual QSO host galaxies. Kellermann et al. (1989) detected most of the low-redshift ($z < 0.5$) Palomar Bright Quasar Survey (PBQS) QSOs at 5 GHz and found a bimodal spectral luminosity *distribution* (not *function*) peaking at $\log[L_5(\text{W Hz}^{-1})] \sim 26$ and ~ 22 . The low-luminosity peak for QSOs spans the range $0.1 < R < 1$ with a median $\langle R \rangle \sim 0.3$. Miller et al. (1993) used high-resolution radio images and [O III] spectra of the PBQS QSOs as evidence for a circumnuclear starburst contribution to the low-luminosity peak. Recent results from significantly more sensitive Karl G. Jansky Very Large Array (VLA) observations of 179 SDSS (Sloan Digital Sky Survey) QSOs in the redshift range $0.2 < z < 0.3$ found a low-luminosity peak (Kimball et al. 2011) centered on $\log[L_6(\text{W Hz}^{-1})] \approx 22.4$ and $R \approx 0.3$ at $\nu = 6 \text{ GHz}$. The radio sources contributing to this peak have a median spectral index $\alpha = -0.7$ consistent with starburst radio emission. Unfortunately their median flux densities are only $\langle S \rangle \approx 0.13 \text{ mJy}$ at 6 GHz and $\langle S \rangle \approx 0.33 \text{ mJy}$ at 1.4 GHz, so making follow-up observations will be difficult. The Kimball et al. (2011) radio luminosity function suggests that most radio sources with $\log[L_6(\text{W Hz}^{-1})] > 23$ at 6 GHz (or $\log[L_{1.4}(\text{W Hz}^{-1})] > 23.4$ at 1.4 GHz) in low-redshift QSOs are powered primarily by AGNs, not starbursts.

Kellermann et al. (1994) reobserved “radio quiet” QSOs and low-luminosity AGNs from their BQS sample (Kellermann et al. 1989) at 5 GHz with $18''$ and $0''.5$ resolution and resolved a number of compact cores and extended lobes similar to those in radio-loud quasars, suggesting that central engines exist in galaxies and quasars over a wide range of radio luminosity. They noted, however, that their resolved “radio quiet” QSOs had radio luminosities well in excess of that expected from the underlying galaxy.

Several high-resolution radio observations have demonstrated that most mJy-level radio sources in QSOs contain radio components so compact that they must be AGN-powered. Three flat-spectrum ($\alpha > -0.5$) “radio intermediate” (defined by $10 < R < 250$ at $\nu = 5 \text{ GHz}$) QSOs were found to have brightness temperatures $T_b > 10^9 \text{ K}$ (Falcke et al. 1996), much too high for starburst radio emission. However, only one of them (PG 1309+355 at $z = 0.184$) satisfies our $M_B < -23$ criterion for a QSO, and its 5 GHz radio luminosity $\log[L_5(\text{W Hz}^{-1})] \approx 24.6$ is an order of magnitude higher than the most luminous starburst yet found in a low-redshift QSO. Blundell & Beasley (1998) imaged 12 “radio-quiet quasars” with the VLBA and found strong

evidence for jet-producing central engines in eight of them. However, four of the “quasars” are low-luminosity AGNs with $M_B > -23$ (Mrk 335, III Zw 2, Mrk 705, and II Zw 171). Five of the eight true QSOs were detected by the VLBA, but all five have radio luminosities in the range $23.8 < \log[L_{1.4}(\text{W Hz}^{-1})] < 26.2$ high enough that we expect a significant AGN contribution. Ulvestad et al. (2005) considered a sample of 11 “radio-quiet quasars” having total 5 GHz flux densities of 4 mJy or greater. Three have no compact cores stronger than 1 mJy and were discarded from the sample. New VLBA images were made of five, one of which (UGC 09412) is a low-luminosity AGN. Two of the true quasars are in the Blundell & Beasley (1998) sample above. The remaining QSOs (J0804+6459 at $z = 0.148$ and UM 275 at $z = 2.137$) have radio luminosities $\log[L_5(\text{W Hz}^{-1})] = 23.8$ and 26.0 , respectively, and 5 GHz radio/optical flux ratios $R = 3$ and 22 , respectively, much higher than we expect for radio sources powered only by starbursts. We believe their conclusion “Thus, the most likely explanation for their radio properties is simply the radio-quiet quasars are similar to their ‘traditional’ radio-loud cousins but have less powerful radio jets.” (Ulvestad et al. 2005) applies only to QSOs containing radio sources stronger than starbursts produce. We conclude that, unfortunately, VLB observations are simply not sensitive enough ($\sigma \ll 0.1$ mJy) to address the question of starburst radio emission in large samples of radio-quiet quasars.

Finally, Barvainis et al. (2005) compared radio variability in samples of radio-quiet (defined by having $R < 3$), radio-intermediate, and radio-loud quasars. They found that radio variability is independent of radio loudness. Of the 11 “radio-quiet quasars” monitored, four are low-luminosity AGNs (Mrk 335, Mrk 1148, UGC 11763, and PGC 070504). Four of the seven true QSOs are variable radio sources and three are not. Among the variable QSOs, only PG 0052+251 at $z = 0.155$ is sufficiently radio quiet ($\log[L_8(\text{W Hz}^{-1})] = 22.6$ and $R \sim 0.3$) that a starburst might have contributed significantly to its radio emission. This single source is consistent with the 6 GHz radio luminosity functions shown in Figure 6 of Kimball et al. (2011), which suggests that about one in four QSO radio sources with $\log[L_6(\text{W Hz}^{-1})] = 22.6$ should be AGN-dominated. We believe their conclusion “...the radio emission from radio-quiet quasars originates in a compact structure intimately associated with the active nucleus. The alternative hypothesis, that the emission from radio-weak quasars is from a starburst, is ruled out.” (Barvainis et al. 2005) has been justified only for radio sources stronger than $\log[L_8(\text{W Hz})] \sim 24$ and $R > 1$ in QSOs, not for the weaker radio sources expected from starbursts.

1.5. Outline of This Paper

QSOs have such broad radio luminosity functions that their radio emission can be characterized only via large unbiased samples of radio-detected QSOs. Sensitive directed searches for radio emission from QSOs have been impeded by the small numbers of radio detections. A typical VLA observing program might target $N \sim 100$ QSOs. Detecting statistically useful numbers $N \sim 100 \gg N^{1/2}$ of radio sources requires either a de-

tection rate near 100% or a much larger QSO sample if the detection rate is low (e.g., $N \sim 1000$ if the detection rate is only $\sim 10\%$).

Furthermore, nearby QSOs in which starburst-powered radio sources can be detected individually have such a low sky surface density that a statistically useful sample can be obtained only from an optical survey covering more than a steradian with uniformly accurate multicolor photometry. The SDSS DR7 (Data Release 7) QSO sample (Schneider et al. 2010) covers $\Omega \approx 2.66$ sr at Galactic latitudes $|b| > 30^\circ$ and satisfies that requirement. This paper is based on NRAO VLA Sky Survey (NVSS) (Condon et al. 1998) 1.4 GHz flux densities of (1) a volume-limited sample of 1313 DR7 QSOs with $0.2 < z < 0.45$ (Sec. 2) and (2) a magnitude-limited sample of 2471 DR7 QSOs in the redshift range $1.8 < z < 2.5$ (Sec. 3).

Above the NVSS catalog limit $S \approx 2.4$ mJy beam $^{-1}$, the detection rate in each sample is only about 10%, but the QSO samples are large enough to yield hundreds of NVSS detections. In addition, most of the remaining QSOs can be detected statistically on the NVSS images at levels $S \sim 0.1$ mJy beam $^{-1}$. The main result of the direct detections is that the differential luminosity function $\rho_m(L)$ of strong radio sources powered by the AGNs in QSOs is an extremely flat power law, so flat that extrapolating to lower luminosities predicts essentially no statistical detections at the $S \sim 0.1$ mJy level. Our high statistical detection rate implies a “bump” in the radio luminosity function of QSOs in the range $\log[L(\text{W Hz}^{-1})] \sim 23$ to 24 , depending on redshift. We attribute this bump to radio emission powered by luminous starbursts in the host galaxies of *most* bright QSOs (Sec. 5).

2. THE VOLUME-LIMITED $0.2 < z < 0.45$ QSO SAMPLE

The SDSS DR7 QSO catalog (Schneider et al. 2010) is complete to $i = 19.1$ mag over a solid angle $\Omega = 2.66$ sr around the North Galactic Pole. It contains the small sample of 179 color-selected QSOs defined by $M_i < -23$ in the narrow redshift range $0.2 < z < 0.3$ studied by Kimball et al. (2011) and the larger sample of 1313 QSOs in the wider redshift range $0.2 < z < 0.45$ discussed here. Note that these magnitudes were calculated for an $H_0 = 71$ km s Mpc $^{-1}$ Λ CDM cosmology, so our QSO cutoff corresponds to $M_B \approx -23.8$ for comparison with Schmidt & Green (1983) and should discriminate against the low-luminosity QSOs that can appear in spiral galaxies (Dunlop et al. 2003). Both samples are strictly volume limited because any $M_i < -23$ QSO with $z < 0.45$ is brighter than $i = 19$ mag. There are no more color-selected QSOs with $0.2 < z < 0.45$ to be found in that 21% of the sky, so no observation made at this time and place in the universe can reduce our statistical errors by more than about a factor of two—our sample variance is approaching the “cosmic variance” limit set by the finite observable volume of the universe (Kamionkowski & Loeb 1997).

2.1. Sources in the NVSS Catalog

The entire DR7 area is covered by the NVSS, whose source catalog is complete for statistical purposes above a peak flux density $S_p \approx 2.4$ mJy beam $^{-1}$ at 1.4 GHz.

In the redshift range $0.2 < z < 0.45$ the 45 arcsec FWHM (full width between half-maximum points) beam of the NVSS spans 150 to 250 kpc, more than enough to cover the host galaxy of stars and most of the extended radio emission powered by an AGN. Consequently the NVSS sees most QSOs as point sources and the NVSS integrated flux-density limit is $S \approx S_p = 2.4$ mJy. For radio sources with spectral index $\alpha \approx -0.7$, the corresponding $\nu = 1.4$ GHz (in the source frame) NVSS spectral-luminosity detection limits range from $\log[L_\nu(\text{W Hz}^{-1})] = 23.4$ at $z = 0.2$ to 24.2 at $z = 0.45$. Thus most of these sources are too luminous to be powered primarily by starbursts.

To ensure completeness even for radio sources larger than the NVSS beam, we examined all NVSS catalog entries within 120 arcsec of each QSO. We rejected components centered more than a few arcsec from the optical position unless their morphologies in the NVSS and/or higher-resolution (5.4 arcsec FWHM) FIRST (Becker, White, & Helfand 1995) images plausibly link them with the QSO. Unresolved or symmetric NVSS sources are easily identified with QSOs by radio-optical position coincidence alone, but asymmetric multicomponent sources can be difficult. For example, the left panel of Figure 1 shows two marginally resolved NVSS components whose centers straddle the optical position (cross) of SDSS J091205.16+543141.2. Two lobes and a core are clearly resolved in the FIRST image (right panel), confirming the otherwise uncertain NVSS identification. Because the NVSS has low resolution, it has high surface-brightness sensitivity. The two NVSS components contain essentially all of the QSO flux density, 23.8 mJy, while the three FIRST components add up to only 6.6 mJy. This example illustrates how the NVSS and FIRST complement each other for identifying extended radio sources and measuring their flux densities.

We also found that the FIRST peak flux densities of QSOs fainter than $S \approx 10$ mJy are usually close to the NVSS flux densities, and very few faint NVSS sources are not in the FIRST catalog. This indicates that most of the fainter radio sources produced by these QSOs have half-power linear sizes $\lesssim 5$ kpc and the likelihood that the NVSS has resolved out any faint sources is small. Unfortunately, radio sources powered by starbursts and by low-luminosity jets from AGNs are both consistent with this size limit; sub-arcsecond resolution is needed to distinguish between them (Condon et al. 1991). FIRST probably does not resolve out many sources in the $1 < S(\text{mJy}) < 2.4$ range either, but we have not included the FIRST flux densities for these sources in our statistical analysis because they are systematically low by about 0.25 mJy owing to “snapshot” bias (White et al. 2007). Also the FIRST source count (White et al. 1997) indicates a rapid fall in differential completeness below $S \approx 2$ mJy. Although the NVSS image noise is higher, the snapshot bias is lower, so we chose to study all sources fainter 2.4 mJy statistically via their amplitude distribution on NVSS images (see Section 2.5 for a complete discussion of snapshot bias in FIRST and NVSS) instead.

A number of stronger sources are clearly resolved by the NVSS, but most have brightnesses well above the $2.4 \text{ mJy beam}^{-1}$ NVSS catalog limit. Thus the NVSS integrated flux densities of radio-loud QSOs should be

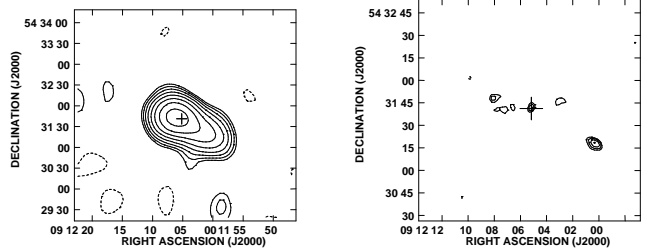


Figure 1. NVSS (left panel) and FIRST (right panel) images of SDSS J091205.16+543141.2 (cross). Contours are separated by factors of $\pm 2^{1/2}$ starting at 1 mJy beam^{-1} (NVSS) and $0.5 \text{ mJy beam}^{-1}$ (FIRST).

accurate and the NVSS should not have missed any radio-loud QSOs. There are 163 NVSS detections with $0.2 < z < 0.45$ (Table 1), of which only 37 are in the narrow redshift range $0.2 < z < 0.3$ that was also covered by our more sensitive directed VLA observations at 6 GHz (Kimball et al. 2011).

2.2. The 1.4 GHz Flux-density Distribution of QSOs Stronger Than 2.4 mJy

Let $n(S)dS$ be the differential number of sources per steradian in the flux-density range S to $S + dS$. Then the brightness-weighted count $S^2 n(S)$ is proportional to the contribution dT_b of sources in each logarithmic flux-density range to the sky background temperature:

$$\left[\frac{dT_b}{d \log(S)} \right] = \left[\frac{\ln(10)c^2}{2k_B \nu^2} \right] S^2 n(S). \quad (4)$$

The brightness-weighted count of all extragalactic sources at 1.4 GHz (mostly radio galaxies) is shown by the upper curve in Figure 2. The lower curve in Figure 2 shows that (1) the 1.4 GHz flux-density distribution of the $0.2 < z < 0.45$ QSOs is a smooth power law above 2.4 mJy and (2) the QSO detection rate grows very slowly with improvements in sensitivity. In the flux-density range $2.4 < S(\text{mJy}) < 1000$, the unbinned maximum-likelihood power-law fit (Crawford et al. 1970) to the brightness-weighted differential source count of these QSOs is $S^2 n(S) = (5.0 \pm 0.4) \times S^{0.80 \pm 0.02} \text{ Jy sr}^{-1}$; that is,

$$n(S) \propto S^{-\beta}, \quad (5)$$

where $\beta = 1.20 \pm 0.02$ is much lower than the static Euclidean $\beta = 2.5$. The Kolmogorov-Smirnov (K-S) test for goodness of fit yields the probability $P > 0.33$ that the source count is consistent with the power-law fit. There are no gaps or other features in this QSO flux-density distribution to suggest more than one source population above $S = 2.4$ mJy, where we expect primarily AGN-dominated radio emission.

Because the flux-density range spanned by these QSOs is large, it is also useful to consider the number $n_{10}(S)$ of radio sources in each logarithmic flux-density interval centered on S . We define n_{10} by

$$n_{10}(S) d \log S = n(S) dS \quad (6)$$

so that

$$n_{10}(S) = \ln(10) S n(S) \propto S^{1-\beta}. \quad (7)$$

For our $0.2 < z < 0.45$ QSOs, $(1-\beta) = -0.20 \pm 0.02$. The QSO counts are “flat” in the sense that $n_{10}(S)$ is nearly

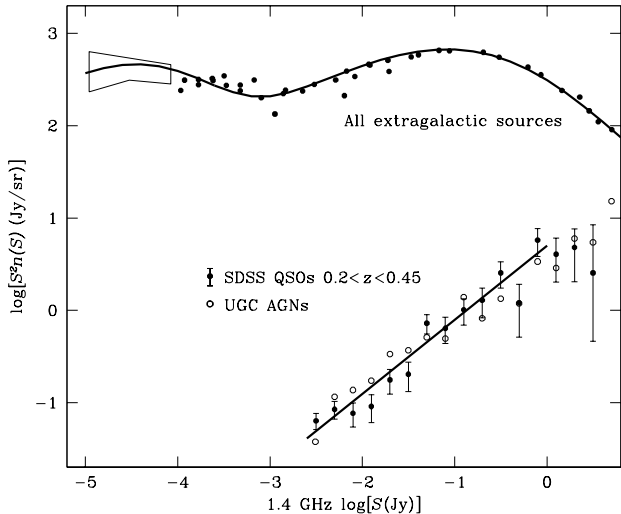


Figure 2. The peaks in the brightness-weighted count $S^2 n(S)$ of all extragalactic sources (Condon & Mitchell 1984; Mitchell & Condon 1985) near $\log[S(\text{Jy})] = -1$ and $\log[S(\text{Jy})] = -4$ match the expected contributions from AGNs (primarily in radio galaxies) and star-forming galaxies, respectively, at typical redshifts $z \sim 1$. The low-redshift SDSS QSO count (filled points with error bars) is well fit by the power-law (solid line) whose slope also matches the count (open circles) of nearby ($z \lesssim 0.05$) UGC galaxies whose radio sources are powered primarily by AGNs (Condon, Cotton, & Broderick 2002). All points in this figure are on the same ordinate scale, so the vertical separation between the points for all extragalactic sources near the top and SDSS QSOs with $0.2 < z < 0.45$ near the bottom shows how the fraction of all radio sources that are in low-redshift QSOs drops from about 1% near $S = 1$ Jy to about 0.01% near $S = 1$ mJy. The nearly equal densities of SDSS QSOs and UGC galaxies is only a coincidence. Abscissa: \log 1.4 GHz flux density (Jy). Ordinate: Differential source count $n(S)$ multiplied by S^2 (Jy sr^{-1}).

independent of S . In each successively lower decade of flux density, the expected number of radio detections rises by only $\text{dex}(0.2) - 1 \approx 60\%$. This is quite different from the “steep” counts of radio galaxies or of all sources in a static Euclidean universe, where $(1 - \beta) \sim -1.5$ regardless of the luminosity function, and the number of radio detections should increase by about 3000% per decade.

The brightness-weighted count of our $0.2 < z < 0.45$ QSOs clearly peaks at the highest flux densities (Figure 2). The strongest 12 radio sources (those with $S > 900$ mJy) comprise only 1% of the 1313 QSOs but contribute more than half of the total radio flux density from the whole sample, even if all 1148 radio sources not in the NVSS catalog had flux densities equal to their $5\sigma = 2.4$ mJy NVSS upper limits.

2.3. The 1.4 GHz Luminosity Function and its Evolution, $0.2 < z < 0.45$

The 1.4 GHz spectral luminosity distribution of QSOs in our sample is shown in Figure 3 as a function of the comoving volume in $\Omega = 2.66$ sr between the redshift cutoff at $z = 0.2$ and the redshift of each QSO. The QSO sample is strictly volume limited and the radio detections are complete above the $S = 2.4$ mJy NVSS limit indicated by the curved line. Consequently the plotted density of points above the curved line is proportional to the 1.4 GHz spectral luminosity function

$$\rho_m(L_\nu) \equiv \ln(m) L_\nu \rho(L_\nu), \quad (8)$$

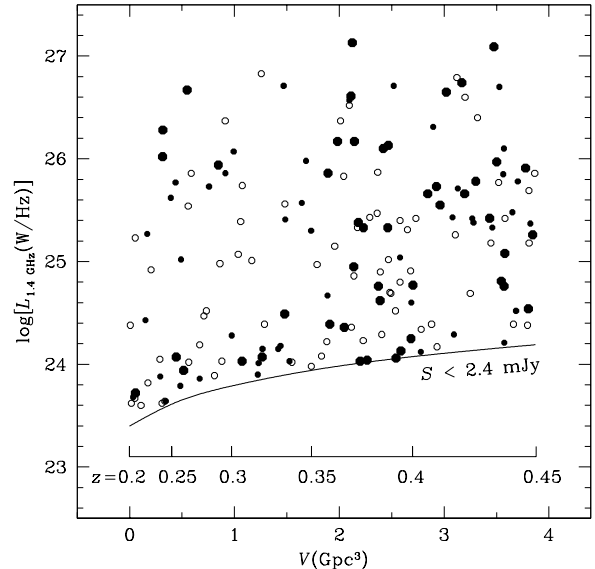


Figure 3. The 1.4 GHz luminosity distribution of QSOs detected by the NVSS is shown as a function of the volume enclosed between the redshift of each QSO and the sample’s lower redshift limit $z = 0.2$. The $S = 2.4$ mJy NVSS sensitivity limit is indicated by the curve. The QSO sample is volume limited, so the density of points above the curve is proportional to its 1.4 GHz luminosity function. Symbols distinguish QSOs by their absolute magnitudes: large filled symbols for $M_i < -24$, small filled symbols for $-24 < M_i < -23.5$, and open symbols for $-23.5 < M_i < -23$. Abscissa: comoving volume V (Gpc^3). Ordinate: \log 1.4 GHz spectral luminosity. Parameter: redshift z .

where $m \equiv \text{dex}(0.4) = 1$ “magnitude” and $\rho(L_\nu) dL_\nu$ is the comoving space density of sources in the spectral luminosity range L_ν and $L_\nu + dL_\nu$. The QSOs in Figure 3 have been grouped into three absolute-magnitude bins: $M_i < -24$ (large filled symbols), $-24 < M_i < -23.5$ (small filled symbols), and $-23.5 < M_i < -23$ (open symbols).

Figure 3 shows that: (1) The 1.4 GHz spectral luminosity function has no statistically significant features (regions of significantly low or high density) in the sampled range $24 < \log[L_{1.4 \text{ GHz}} (\text{W Hz}^{-1})] < 27$ at any redshift $0.2 < z < 0.45$. (2) The radio and optical luminosities do not appear to be correlated. However, the radio luminosities span three decades, while only five of the 163 QSOs are brighter than $M_i = -25.5$, one decade brighter than the $M_i = -23$ optical cutoff, so a linear correlation would be difficult to discern even if there were one. The fact that a linear correlation would be difficult to discern suggests that studying radio/optical ratios R (Schmidt 1970) instead of flux densities S is not likely to yield new insights into low-redshift optically selected QSOs. We note that Mahony et al. (2012) also found no correlation of radio and optical luminosities in their sample of low-luminosity X-ray selected QSOs. (3) The plotted density of points increases to the right, indicating radio density evolution.

We calculated the 1.4 GHz spectral luminosity function of color-selected QSOs brighter than $M_i = -23$ in the redshift range $0.2 < z < 0.45$ using the standard $1/V_{\text{max}}$ method. If there are N sources in the logarithmic bin of

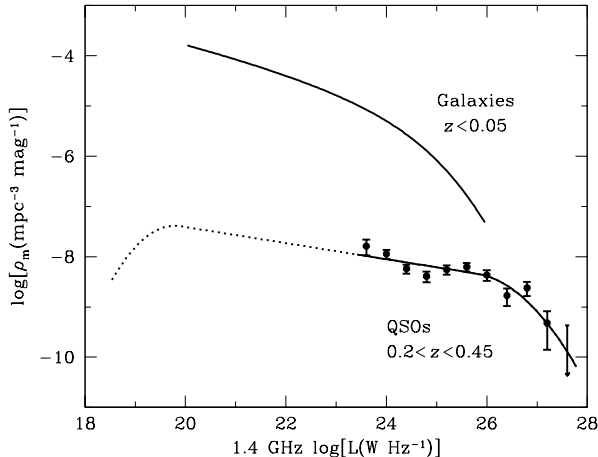


Figure 4. The 1.4 GHz luminosity function of QSOs in the redshift range $0.2 < z < 0.45$ based on NVSS detections is shown by data points at $\log[L_{1.4\text{GHz}}(\text{W Hz}^{-1})] = 23.6$ to 27.2 by 0.4 and an upper limit at 27.6 . The continuous curve approximating the QSO data follows equations 11 and 13. The dotted line is a power-law extrapolation to lower luminosities, cut off below $\log[L_{1.4\text{GHz}}(\text{W Hz}^{-1})] \sim 20$ to ensure that the number of radio sources equals the number of QSOs. Abscissa: log 1.4 GHz spectral luminosity (W Hz^{-1}) . Ordinate: log comoving space density (Mpc^{-3}) of sources per “magnitude” = dex(0.4) luminosity range.

width m centered on spectral luminosity L_ν , then

$$\rho_m(L_\nu) = \sum_{i=1}^N \left(\frac{1}{V_{\max}} \right)_i, \quad (9)$$

where V_{\max} is the comoving volume in the sample solid angle $\Omega = 2.66$ sr between the minimum redshift $z = 0.2$ and the maximum redshift $z_{\max} \leq 0.45$ at which the source could have been detected. The rms statistical uncertainty of $\rho_m(L_\nu)$ is

$$\sigma = \left[\sum_{i=1}^N \left(\frac{1}{V_{\max}} \right)_i^2 \right]^{1/2}. \quad (10)$$

The binned luminosity function of QSOs averaged over the redshift range $0.2 < z < 0.45$ is shown in Figure 4. The data points can be fit by the power law

$$\log[\rho_m(\text{mag}^{-1} \text{Mpc}^{-3})] = -4.21 - 0.16 \log[L_{1.4\text{GHz}}(\text{W Hz}^{-1})] \quad (11)$$

in the luminosity range $23.4 < \log[L_{1.4\text{GHz}}(\text{W Hz}^{-1})] < 25.8$. The power-law slope

$$\epsilon \equiv d \log(\rho_m) / d \log(L_\nu) = -0.16 \quad (12)$$

is close to the slope $(1-\beta) \approx -0.2$ of $n_{10}(S)$, as suggested in Section 2.2. It is somewhat flatter than the luminosity function of UGC radio galaxies powered by AGNs (upper curve in Figure 4).

At higher luminosities, the luminosity function must fall below this flat power law; otherwise the spectral power density contributed by the most luminous sources would diverge. The amount $\Delta \log(\rho_m)$ by which the observed luminosity function falls below the power-law fit can be approximated by the (somewhat arbitrary, but simple and yielding a satisfactory fit to the limited data)

quadratic form indicated by the lower continuous curve in Figure 4:

$$\Delta \log[\rho_m(\text{mag}^{-1} \text{Mpc}^{-3})] = - \left[(\log[L_{1.4\text{GHz}}(\text{W Hz}^{-1})] - 25.8) / 1.6 \right]^2 \quad (13)$$

when $\log[L_{1.4\text{GHz}}(\text{W Hz}^{-1})] > 25.8$. Finally, the total number of optically selected QSOs is finite ($N = 1313$ over $\Omega = 2.66$ sr in the redshift range $0.2 < z < 0.45$), so the total number of radio sources predicted by the luminosity function should not exceed this number. Any extrapolation of the fitted luminosity function to lower luminosities (dotted line in Figure 4) must cut off below $\log[L_{1.4\text{GHz}}(\text{W Hz}^{-1})] \sim 20$ prevent the total number of radio sources from exceeding the number of QSOs.

The NVSS catalog should contain all sources with spectral luminosities $\log[L_{1.4\text{GHz}}(\text{W Hz}^{-1})] > 24.2$ throughout the redshift range $0.2 < z < 0.45$. Low-redshift radio sources this strong are probably dominated by emission from AGNs, not starbursts. The evolution of their luminosity function with redshift may be characterized in terms of pure density evolution (shifting the luminosity function horizontally in Figure 4)

$$\log[\rho_m(L, z)] = \log[g(z)\rho_m(L, 0)] \quad (14)$$

or pure luminosity evolution (shifting the luminosity function vertically in Figure 4)

$$\log[\rho_m(L, z)] = \log[\rho_m(L/f(z), 0)], \quad (15)$$

where the functions $g(z)$ and $f(z)$ specify the amounts of density and luminosity evolution, respectively. For power-law density evolution $g(z) = (1+z)^\delta$, $\delta = +6.0 \pm 1.8$ is needed to match the 1.4 GHz data in this portion of the redshift–luminosity plane, and the fit is satisfactory [$P(\chi^2) > 0.2$]. Thus the evolving 1.4 GHz luminosity function of QSOs in the redshift range $0.2 < z < 0.45$ is well approximated by replacing Equation 11 with

$$\log[\rho_m(\text{mag}^{-1} \text{Mpc}^{-3})] = -5.06 - 0.16 \log[L_{1.4\text{GHz}}(\text{W Hz}^{-1})] + 6.0 \log(1+z) \quad (16)$$

and leaving the cutoff Equation 13 unchanged.

Pure luminosity evolution of the form $f(z) = (1+z)^\lambda$ is indistinguishable from pure density evolution in the power-law portion of a luminosity function. However, the small power-law slope $\epsilon \approx -0.16$ of the QSO luminosity function means that very strong luminosity evolution is needed to have the same effect as moderate density evolution: $\lambda \sim -\delta/\epsilon \sim 38$. The high-luminosity cutoff cannot evolve this rapidly because there are only two sources with $\log[L_{1.4\text{GHz}}(\text{W Hz}^{-1})] > 26$, so pure luminosity evolution does not fit our radio data.

2.4. Why is the QSO Flux-density Distribution So Flat?

The flat flux-density distribution $n_{10}(S)$ of radio sources in low-redshift optically selected QSOs does not prove that they are significantly different from the radio sources in nearby optically selected galaxies. The open circles in Figure 2 show the weighted count $S^2 n(S)$ of AGN-dominated radio sources in low-redshift ($z \lesssim 0.05$) UGC galaxies (Condon, Cotton, & Broderick 2002); their power-law slope is almost the same. (Their

sky density is also nearly the same, but that is just a coincidence that depends on the size of the UGC sample.)

Why do these optically selected QSO and galaxy samples have such flat 1.4 GHz flux-density distributions? Consider the flux-density distributions in two extreme cases: (1) In an infinite static Euclidean universe, the slope of $n_{10}(S)$ would be $1 - \beta = -1.5$, for any luminosity function. (2) If all of the sources in a sample were at exactly the same distance, the slope of $n_{10}(S)$ would equal the slope of the luminosity function $\rho_m(L)$. For the more realistic case of a sample of sources spanning a finite redshift range z_{\min} to z_{\max} , the flux-density distribution will be the convolution of the luminosity function with a smoothing function whose width is roughly $(z_{\max}/z_{\min})^2$, the range of flux densities for a source of fixed luminosity as it is moved across the redshift range.

For both the SDSS QSO and UGC galaxy samples, the power-law portions of their 1.4 GHz luminosity functions (Figure 4) are much wider than $(z_{\max}/z_{\min})^2 \sim 6$ for steep-spectrum QSOs confined to $0.2 < z < 0.45$. About 7/8 of the volume in $0 < z < 0.05$ containing the AGN-dominated UGC galaxies is in the narrow redshift range $0.025 < z < 0.05$ for which the smoothing width is only ≈ 4 . In the small-smoothing limit, the power-law slope $(1 - \beta)$ of n_{10} naturally approaches the power-law slope $d \log(\rho_{10})/d \log L_\nu$ of the differential luminosity function expressed as a source density per log radio luminosity. Thus the flat and nearly equal flux-density distributions of both the SDSS QSO and the AGN-dominated UGC galaxy samples are telling us only that both samples have relatively broad and flat radio luminosity functions. If the AGN-powered radio sources in both optically selected samples are intrinsically similar, we should *expect* our QSOs to have a distinctly sub-Euclidean flux-density distribution.

The observed $\beta \approx 1.2$ is also consistent with relativistic beaming, which tries to make $\beta \approx 4/3$ (Scheuer & Readhead 1979). However, relativistic beaming of the modestly luminous {typical $\log[L_{1.4\text{GHz}}(\text{W Hz}^{-1})] \sim 25$ } NVSS radio sources in our low-redshift QSO sample is probably insufficient to influence the radio flux-density distribution. In beaming models, the most luminous sources are the most highly beamed, so that most of their flux densities arise in highly relativistic ($\gamma \sim 5\text{--}10$) components approaching within $\sim \gamma^{-1}$ radians of our line of sight. Relativistic jets are compact and one-sided, but the most luminous sources in our sample are not. Table 1 lists 26 sources with (apparent) $\log[L_{1.4\text{GHz}}(\text{W Hz}^{-1})] > 26$, but only seven have even half of their flux density unresolved by FIRST; the rest are too extended (linear diameter $\gtrsim 5$ kpc) and centered on their optical QSO positions to be strongly boosted. The seven fairly compact sources contribute only 34% of the total apparent luminosity of the 26 luminous sources, so removing them would reduce the total luminosity of the sample by at most $\Delta \log(L_\nu) = -0.18$. What we see is what we get, and we can calculate reasonably accurate intrinsic luminosities and luminosity functions by assuming isotropic radio emission.

2.5. NVSS Statistical Detections: Numerous Faint Sources Powered by Star Formation?

To detect radio sources weaker than $S = 2.4$ mJy, we originally measured NVSS peak flux densities at the positions of all $N = 179$ color-selected QSOs in the narrow redshift band $0.2 < z < 0.3$ (Kimball et al. 2011). The NVSS image noise has a nearly Gaussian amplitude distribution with rms $\sigma = 0.45 \pm 0.01$ mJy beam $^{-1}$ and zero mean (Condon et al. 1998). A starburst with luminosity $\log(L/L_\odot) \approx 11$ obeying the FIR/radio correlation should produce a radio source with spectral index $\alpha \approx -0.7$ and spectral luminosity $\log[L_\nu(\text{W Hz}^{-1})] \approx 22.5$ at $\nu = 1.4$ GHz in the source frame. Such a source would yield an observed 1.4 GHz flux density ranging from $S = 0.12$ mJy at $z = 0.3$ to $S = 0.30$ mJy at $z = 0.2$. The NVSS is not sensitive enough to detect such faint sources individually, but the distribution of peak flux densities on QSO positions can be used to detect a large ($N > 100$) sample of them statistically.

White et al. (2007) discovered a potential problem with statistical detections: the nonlinear CLEAN bias associated with the high dirty-beam sidelobes of snapshot surveys like FIRST and NVSS can produce a “snapshot bias” that lowers the image peak flux densities of sources fainter than the catalog limit. The snapshot bias for a faint source is about 40% of the peak flux density on a FIRST image. To see if snapshot bias might affect the peak flux densities of faint QSOs on NVSS images, we followed their technique and measured NVSS peak flux densities on the positions of faint sources found in the sensitive ($\sigma \approx 0.023$ mJy beam $^{-1}$) 1.4 GHz VLA image covering the Spitzer First-Look Survey (Condon et al. 2003). This image was made from data having very good (u, v) -plane coverage, so its snapshot bias should be extremely low. The results of this comparison are listed in Table 2. They show that the NVSS snapshot bias is too small to measure over the flux-density range $0.115 < S_p < 0.460$ mJy beam $^{-1}$.

Figure 5 shows the distribution of NVSS peak flux densities S_p at the optical positions of the 179 QSOs with $0.2 < z < 0.3$ (continuous histogram) and at the 179 “blank sky” positions exactly one degree north of the QSOs (dotted histogram). The blank-sky distribution is well fit by a Gaussian with mean $\langle S_p \rangle = 0.00 \pm 0.04$ mJy beam $^{-1}$ and rms $\sigma = 0.48 \pm 0.04$ mJy beam $^{-1}$ (dotted curve) consistent with NVSS image fluctuations. The whole distribution of peak flux densities on the QSO positions is clearly displaced from zero and has a long positive tail, indicating that the NVSS has detected most $0.2 < z < 0.3$ QSOs statistically at typical peak flux densities $S_p \sim 0.3$ mJy beam $^{-1}$, which corresponds to an average spectral luminosity $\log[L_{1.4\text{GHz}}(\text{W Hz}^{-1})] \sim 22.7$ in this redshift range.

Our high detection rate is not consistent with a power-law extrapolation of the flat flux-density distribution of AGN-dominated QSOs, which would yield the dashed curve in Figure 2. The high detection rate of faint sources requires a peak or “bump” in the luminosity function near $\log[L_{1.4\text{GHz}}(\text{W Hz}^{-1})] \sim 22.7$. This bump is confirmed by individual detections of nearly all of the $0.2 < z < 0.3$ QSOs at 6 GHz (Kimball et al. 2011).

We hypothesize that the bump in the QSO luminosity function corresponds to the emergence of the host starburst galaxies as the dominant contributors to the

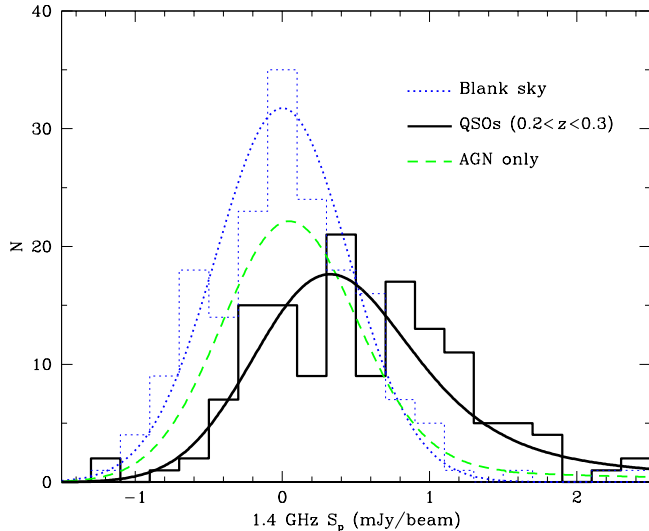


Figure 5. The continuous histogram shows the distribution of NVSS peak flux densities for the volume-limited sample 179 SDSS QSOs in the redshift range $0.2 < z < 0.3$. The dotted histogram (colored blue in the online version) indicates the distribution of NVSS peak flux densities at “blank sky” positions one degree north of the QSOs, and it is well fit by a Gaussian of mean $\langle S_p \rangle = -0.01 \pm 0.04$ mJy beam $^{-1}$ and rms $\sigma = 0.48 \pm 0.04$ mJy beam $^{-1}$ (dotted curve, colored blue in the online version). The dashed curve (colored green in the online version) is the distribution predicted by extrapolating the observed luminosity function of SDSS QSOs to lower luminosities, and the continuous black curve represents the distribution predicted by our best-fit model in which both AGNs and star-forming host galaxies contribute to the radio emission of QSOs.

radio emission. Figure 6 compares the 1.4 GHz luminosity functions of low-redshift ($z < 0.05$) UGC galaxies (Condon, Cotton, & Broderick 2002) whose radio emission is powered primarily by AGNs (continuous green curve) or by recent star formation (continuous red curve) with a simple model for the radio luminosity function of $0.2 < z < 0.3$ QSOs. The continuous black curves in Figures 5 and 6 correspond to our model luminosity function that fits both the NVSS detections and the S_p distribution of nondetections. Our model assumes that the total radio emission of each QSO is the sum of statistically independent AGN- and starburst-powered components. The lower green curve in Figure 6 is similar to the extrapolated luminosity function of Figure 4, constrained by NVSS detections above $\log[L(\text{W Hz}^{-1})] \approx 24$, constrained statistically in the luminosity range $22 < \log[L(\text{W Hz}^{-1})] < 24$ (dashed green line), and at lower luminosities by requiring that the number of radio sources equal the number of QSOs (dotted green curve). The dashed red curve is the radio luminosity function of sources powered by recent star formation in the host galaxies needed to match the observed total luminosity function. The direct detections of faint sources reported in Kimball et al. (2011) match the dashed red curve very well. It suggests that most QSOs host starbursts whose luminosities are comparable with the more luminous starbursts in nearby galaxies. The typical star-formation rate can be estimated from the peak of the dashed red curve: $\log[L_{1.4 \text{ GHz}}(\text{W Hz})] \sim 22.7$ corresponds to a star-formation rate $SFR \sim 20 M_\odot \text{ yr}^{-1}$

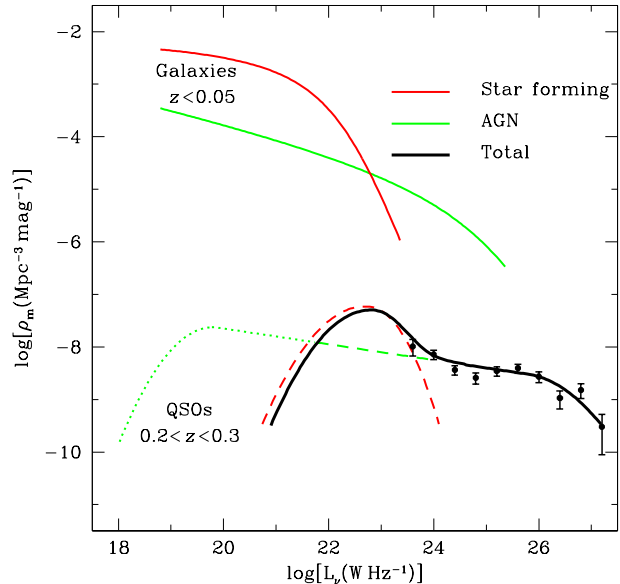


Figure 6. Comparison of the 1.4 GHz luminosity functions of nearby galaxies whose radio sources are powered primarily by star formation (continuous red curve) or by AGNs (continuous green curve) with our model for the luminosity function of $0.2 < z < 0.3$ QSOs (black curve). The data points are from Figure 4 with $\log[\rho_m (\text{Mpc}^{-3} \text{ mag}^{-1})]$ lowered by 0.20 to correct for density evolution (Sec. 2.3). The green dashed line is the power-law extrapolation of the AGN-only contribution, and the green dotted curve shows how this extrapolation might be truncated so the number of AGNs does not exceed the total number of QSOs. The red dashed curve shows the luminosity function of the starbursts only. The black curve is the convolution of the AGN and starburst curves. (Condon 1992).

2.6. Stacking

We note that measuring the full flux-density distribution of undetected QSOs is not the same as “stacking,” which collapses the distribution to a single statistic, the mean value of the peak flux density $\langle S_p \rangle$ of the N QSOs fainter than the catalog limit S_{lim} . The implicit assumptions needed to justify the use of stacking are (1) $\langle S_p \rangle$ is a good statistic for describing the QSO flux-density distribution and (2) stacking divides the error in this mean by about $N^{1/2}$. These assumptions fail if the flux-density distribution is a nearly flat power law, as we found for the cataloged NVSS QSOs. When $n_{10}(S)$ is nearly independent of S , then $n(S) \sim S^{-1}$ and $\langle S_p \rangle$ is dominated by the small number $\eta \ll N$ of sources just fainter than S_{lim} , the fractional statistical uncertainty in $\langle S_p \rangle$ is about $\langle S_p \rangle / \eta^{1/2} \gg \langle S_p \rangle / N^{1/2}$, and $\langle S_p \rangle$ depends more sensitively on the survey limit S_{lim} than on the intrinsic properties of the optically selected QSO sample.

Consider a QSO sample whose differential flux-density distribution is close to $n(S) \propto S^{-1}$ over a wide ($S_{\text{min}} \ll S_{\text{max}}$) flux-density range S_{min} to S_{max} . The value of S_{min} is too low to measure; it is only inferred from the fraction f of detected QSOs and the integral constraint that all QSOs must be stronger than S_{min} . The average flux density $\langle S \rangle$ of unresolved sources (so $S_p \approx S$) in a stack of images with $S < S_{\text{lim}}$ is

$$\langle S \rangle = \frac{\int_{S_{\text{min}}}^{S_{\text{lim}}} S n(S) dS}{\int_{S_{\text{min}}}^{S_{\text{lim}}} n(S) dS} \approx \frac{S_{\text{lim}} - S_{\text{min}}}{\ln(S_{\text{lim}}/S_{\text{min}})} \quad (17)$$

If the fraction f of individually detected sources is not close to unity, then $S_{\text{lim}} \gg S_{\text{min}}$ and the numerator $S_{\text{lim}} - S_{\text{min}} \approx S_{\text{lim}}$. The number of sources per logarithmic flux-density interval is constant between S_{min} and S_{max} when $n(S) \propto S^{-1}$ so

$$\ln\left(\frac{S_{\text{max}}}{S_{\text{lim}}}\right) = f \ln\left(\frac{S_{\text{max}}}{S_{\text{min}}}\right). \quad (18)$$

Using

$$\ln\left(\frac{S_{\text{max}}}{S_{\text{min}}}\right) = \ln\left(\frac{S_{\text{max}}}{S_{\text{lim}}}\right) + \ln\left(\frac{S_{\text{lim}}}{S_{\text{min}}}\right) \quad (19)$$

yields

$$\langle S_p \rangle \approx \frac{S_{\text{lim}}}{(1-f) \ln(S_{\text{max}}/S_{\text{min}})}. \quad (20)$$

The stacking flux density $\langle S_p \rangle$ depends almost linearly on the detection limit S_{lim} and only logarithmically on the intrinsic QSO flux-density distribution. For example, the NVSS detected $f = 37/179 \approx 0.21$ of the DR7 QSOs with $0.2 < z < 0.3$ above $S_{\text{lim}} = 2.4$ mJy. If $S_{\text{max}}/S_{\text{min}} \sim 10^8$, then Equation 20 predicts $\langle S_p \rangle \approx S_{\text{lim}}/15 \approx 0.16$ mJy beam⁻¹, half of which is contributed by the small expected number $\eta \approx 5$ of sources with $S_{\text{lim}}/2 < S < S_{\text{lim}}$.

White et al. (2007) made numerical simulations of stacking with Gaussian and exponential distributions and also concluded that the stack mean does not provide a very robust measurement. They studied the stack median as well, which should be better than the mean because it is less sensitive to the strongest sources. However, their simulations showed that the stack median recovered from exploiting low-SNR data (the usual reason for stacking) approaches the true mean, so they interpreted their stack medians as means.

Mahony et al. (2012) has independently noted several limitations of stacking.

We believe it is both safer and more sensitive to fit a model to the entire amplitude distribution (Figure 5) than to rely on *any* stacking statistic. In particular, if the whole S_p distribution is shifted to positive flux densities, we can conclude that *most* of the QSOs are detectable radio sources.

2.7. Evolution of the Faint Radio Sources, $0.2 < z < 0.45$

Encouraged by our statistical detection of 1.4 GHz emission at starburst luminosities from most of the 179 QSOs with $0.2 < z < 0.3$ and its confirmation by individual detections (Kimball et al. 2011), we measured NVSS peak flux densities at the positions of all 1313 QSOs with $0.2 < z < 0.45$ and divided them into five redshift bins ($0.2 < z < 0.25$, $0.25 < z < 0.3$, $0.3 < z < 0.35$, $0.35 < z < 0.4$, and $0.4 < z < 0.45$) to constrain the evolution of the hypothesized starburst radio emission over lookback times from 2.4 to 4.6 Gyr. The results are shown as histograms in Figure 7. The histogram of peak flux densities in 1313 “blank sky” positions one degree north of the QSOs is plotted in the top panel, and the matching smooth curve shows the Gaussian fit with mean $\langle S_p \rangle = -0.004 \pm 0.013$ mJy beam⁻¹ and rms $\sigma = 0.458 \pm 0.013$ mJy beam⁻¹. The lower five panels

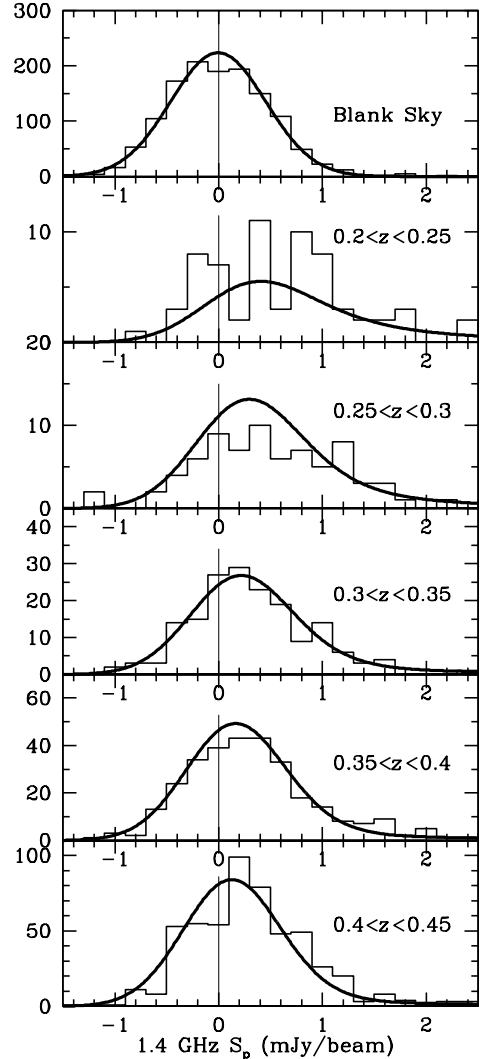


Figure 7. Histograms of NVSS peak flux densities for 1313 SDSS QSOs in five redshift ranges spanning $0.2 < z < 0.45$ fitted with an evolutionary model (smooth curves). The top panel shows the distribution of peak flux densities on “blank sky” reference positions one degree north of the QSOs; it is nearly Gaussian with mean $\langle S_p \rangle = -0.004 \pm 0.013$ mJy beam⁻¹ and rms $\sigma = 0.458 \pm 0.013$ mJy beam⁻¹.

contain the histograms of NVSS peak flux densities at the QSO positions, separated into redshift bins.

The NVSS detection rate in the $0.2 < z < 0.45$ QSO sample is only $163/1313 \approx 12\%$ above 2.4 mJy, so 88% of the 1313 QSOs have $S_p < 2.4$ mJy beam⁻¹ and models that match the numbers of sources in each redshift bin are constrained primarily by the numbers and hence density evolution of the optically selected QSOs. The radio data determine the flux-density distribution within each redshift bin and hence constrain the luminosity evolution of these low-luminosity radio sources.

As in Section 2.3, we describe the density evolution of the optically selected QSOs by $\rho_m(z) \propto (1+z)^\delta$. The best fit, shown by the smooth curves in Figure 7, is for $\delta = +8.5 \pm 2$. The best fit is poor [$P(\chi^2) \sim 0.01$] because the numbers of optically selected QSOs in the redshift

bins $0.2 < z < 0.25$ ($N = 85$) and $0.25 < z < 0.3$ ($N = 94$) are nearly equal but the comoving volumes (0.402 Gpc^3 and 0.572 Gpc^3 , respectively) are not. These numbers favor slightly negative density evolution ($\delta < 0$) in the $0.2 < z < 0.3$ redshift range. The positive value $\delta = +8.5 \pm 2$ for the faint sources over the whole range $0.2 < z < 0.45$ is consistent with the value $\delta = +6.0 \pm 1.8$ for the stronger (primarily AGN-powered) radio sources with $0.2 < z < 0.45$.

If we model 1.4 GHz luminosity evolution of the fainter radio sources by the form $L_\nu(z) \propto (1+z)^\lambda$, the best fit is consistent with no luminosity evolution: $\lambda = -1 \pm 3$.

All of these results are actually consistent with each other and can be summarized as follows: The optically selected QSOs undergo strong density evolution over the redshift range $0.2 < z < 0.45$. Both the weak and strong radio sources undergo a comparably strong density evolution with no detectable luminosity evolution. The likelihood of radio emission at any spectral luminosity from any particular QSO is independent of redshift in the range $0.2 < z < 0.45$. Although the space density of optically selected QSOs evolves dramatically, the likelihood and strength of radio emission from each QSO appears to be independent of redshift.

3. THE MAGNITUDE-LIMITED $1.8 < z < 2.5$ QSO SAMPLE

Many historical QSO samples favor the redshift range $1.8 < z < 2.5$ in which the Ly α line is redshifted to the blue optical band. To test the statistical significance of the Miller et al. (1990) bimodal radio luminosity distribution of such high-redshift QSOs, we chose a magnitude-limited sample of all 2471 color-selected DR7 QSOs brighter than $m_r = 18.5$ in that redshift range. These QSOs are all extremely luminous because our red magnitude limit corresponds to $M_i \approx -26.9$ at $z = 1.8$ and $M_i \approx -27.7$ at $z = 2.5$.

The NVSS detected radio emission stronger than $S = 2.4 \text{ mJy}$ from only 191 (8%) of them (Table 3), consistent with the usual low detection rates at this sensitivity. The brightness-weighted 1.4 GHz flux-density distribution $S^2n(S)$ of the NVSS detections is shown by the points with error bars in the lower part of Figure 8. The power-law fit to their brightness-weighted differential source count is

$$S^2n(S) = (12.9 \pm 1.0) \times S^{0.99 \pm 0.02} \text{ Jy sr}^{-1} \quad (21)$$

in the flux-density range $2.4 < S(\text{mJy}) < 1000$. Once again, the QSO counts are extremely flat in the sense that the number of sources per decade of flux density is nearly constant: $Sn(S) \propto n_{10}(S) \propto S^{-0.01}$. The strongest 13 of the 2471 QSOs ($\approx 0.5\%$) account for more than half of the total radio flux density from the high-redshift QSO sample.

Figure 9 shows the luminosity distribution of these QSOs as a function of the comoving volume beyond $z = 1.8$ in $\Omega = 2.66 \text{ sr}$. Our magnitude-limited high-redshift QSO sample is volume limited for those QSOs brighter than $M_i = -27.7$ (filled points) above the $S = 2.4 \text{ mJy}$ line, where the plotted density of filled points is proportional to the evolving radio luminosity function. In the redshift range $1.8 < z < 2.5$ the density evolution of radio sources stronger than $\log[L(\text{WHz}^{-1})] = 26$ in high-redshift QSOs with $M_i \leq -27.7$ is small or slightly

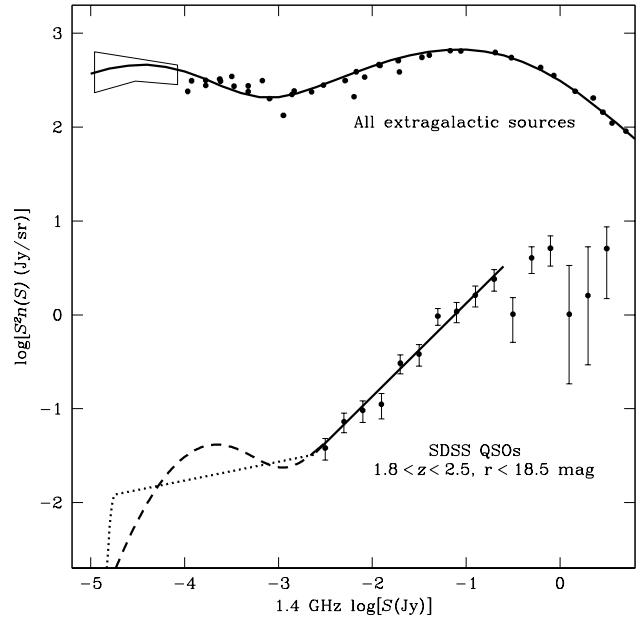


Figure 8. The peaks in the brightness-weighted count of all extragalactic sources near $\log[S(\text{Jy})] = -1$ and $\log[S(\text{Jy})] = -4$ match the expected contributions from AGNs (primarily radio galaxies) and star-forming galaxies, respectively, at typical redshifts $z \sim 1$. The high-redshift SDSS QSO count (filled points with error bars in the lower part of the plot) of sources stronger than the NVSS detection limit $S = 2.4 \text{ mJy}$ is well fit by a power-law (solid line) for which the slope of $S^2n(S)$ is $+0.99 \pm 0.02$. The dashed and dotted curves illustrate the range of faint-source counts needed to match the NVSS peak flux-density distribution on the positions of high-redshift QSOs fainter than 2.4 mJy . Abscissa: \log 1.4 GHz flux density (Jy). Ordinate: Differential source count multiplied by S^2 (Jy sr^{-1}).

negative, as expected: if $\rho_m \propto (1+z)^\delta$, $\delta = -0.3 \pm 1.8$. The correlation of radio and optical luminosities is weak; if anything, the most luminous radio sources are under-represented among the optically most luminous QSOs (large filled points), many of which have radio luminosities near $\log[L(\text{WHz}^{-1})] = 26$. As expected from the 1.4 GHz source count, the 1.4 GHz spectral luminosity function averaged over the $1.8 < z < 2.5$ redshift range is nearly flat (Figure 10) until it cuts off around $\log[L_\nu(\text{WHz}^{-1})] \approx 28.8$, the highest radio luminosity found in this huge (77 Gpc^3) comoving volume.

3.1. NVSS Statistical Detections: Faint Sources Powered Primarily by Star Formation?

Using the technique described in Sec. 2.5, we obtained the NVSS peak flux densities at the positions of all 2471 high-redshift QSOs and at the 2471 “blank sky” positions offset by 1 deg of declination. Figure 11 shows the observed distributions of peak flux densities on the QSO positions (continuous histogram) and on the blank sky points (dotted histogram). The continuous histogram is clearly shifted to the right, indicating that most of the QSOs are weak radio emitters, and their median peak flux density is $\langle S \rangle \approx 0.05 \pm 0.01 \text{ mJy beam}^{-1}$. The blank sky distribution is well approximated by a Gaussian (dotted curve) with mean $\langle S_p \rangle = -0.014 \pm 0.009 \text{ mJy beam}^{-1}$ and rms $\sigma = 0.459 \pm$

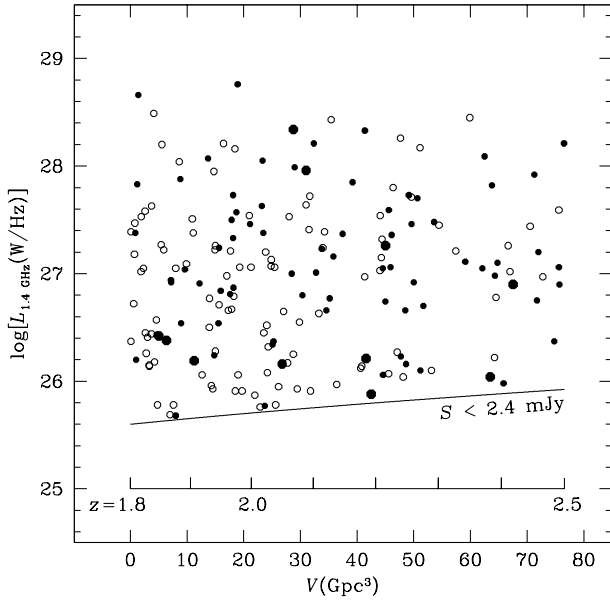


Figure 9. The 1.4 GHz luminosity distribution of QSOs detected by the NVSS is shown as a function of the volume enclosed between the redshift of each QSO and the sample’s lower redshift limit $z = 1.8$. The $S = 2.4$ mJy NVSS sensitivity limit is indicated by the curve. Symbols distinguish QSOs by their absolute magnitudes: large filled symbols for $M_i < -28.7$, small filled symbols for $-28.7 < M_i < -27.7$, and open symbols for $-27.7 < M_i$. The QSO sample is volume limited for QSOs with $M_i < -27.7$ (filled points), so the density of filled points above the curve is proportional to the 1.4 GHz luminosity function of QSOs more luminous than $M_i = -27.7$. Abscissa: comoving volume V (Gpc^3). Ordinate: log 1.4 GHz spectral luminosity. Parameter: redshift z .

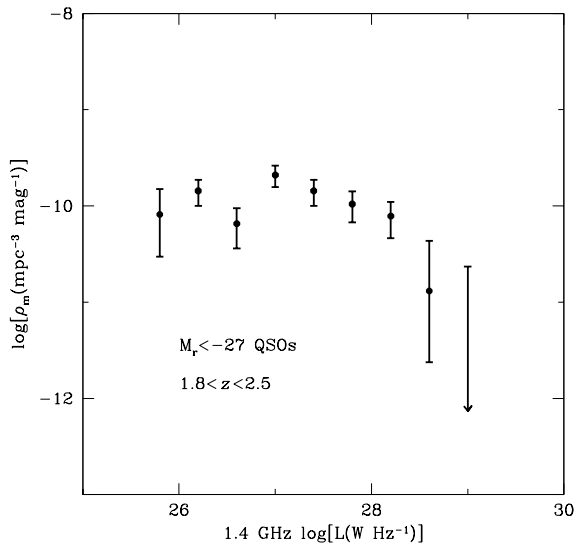


Figure 10. The 1.4 GHz luminosity function of QSOs more luminous than $M_i = -27.7$ in the redshift range $1.8 < z < 2.5$ is shown by data points at $\log[L_{1.4 \text{ GHz}} (\text{W Hz}^{-1})] = 25.8$ to 28.6 by 0.4 and an upper limit at 29.0 . Abscissa: log 1.4 GHz spectral luminosity (W Hz^{-1}). Ordinate: log comoving space density (Mpc^{-3}) of sources per “magnitude” = dex(0.4) luminosity range.

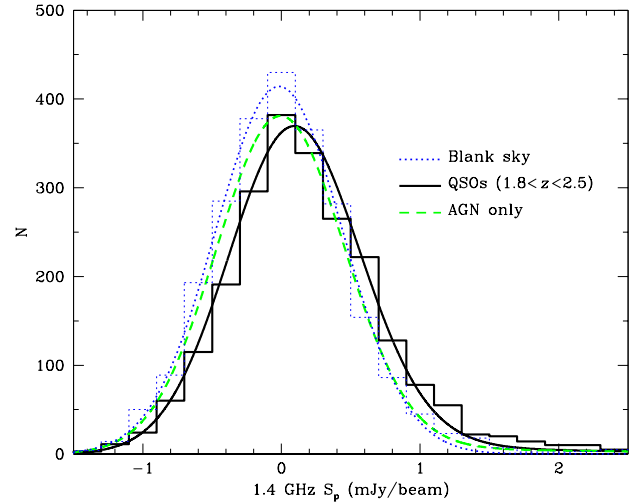


Figure 11. The continuous histogram shows the distribution of NVSS peak flux densities for the magnitude-limited sample of 2471 SDSS QSOs brighter than $m_r = +18.5$ in the redshift range $1.8 < z < 2.5$. The dotted histogram (colored blue in the online version) indicates the distribution of NVSS peak flux densities at “blank sky” positions one degree north of the QSOs, and it is well fit by a Gaussian of mean $\langle S_p \rangle = -0.014 \pm 0.009$ mJy beam $^{-1}$ and rms $\sigma = 0.459 \pm 0.009$ mJy beam $^{-1}$ (dotted curve, colored blue in the online version). The dashed curve (colored green in the online version) is the distribution predicted by extrapolating the flux-density distribution of NVSS sources powered primarily by AGNs to lower luminosities, and the continuous black curve represents the distribution predicted by our best-fit model extremely luminous star-forming host galaxies may contribute significantly to the radio emission of high-redshift QSOs.

0.009 mJy beam $^{-1}$. Simply extrapolating the flat power-law flux-density distribution (Equation 21) of sources so luminous $\{\log[L (\text{W Hz}^{-1})] > 25.8\}$ that they must be powered primarily by AGNs and convolving that flux-density distribution with the blank-sky Gaussian fit yields the dashed curve in Figure 11. The dashed curve is a poor match to the continuous QSO histogram because the extrapolation predicts that the peak flux densities of most QSOs are extremely low (< 0.001 mJy beam $^{-1}$). It is necessary to invoke a rise or peak in the flux-density distribution near $S \sim 0.05$ mJy ($R \sim 0.3$) to explain the high detection rate implied by the positive offset of the QSO histogram.

The dotted line in Figure 8 indicates the weighted faint-source count from the power-law extrapolation that (1) matches with the observed count at 2.4 mJy, (2) satisfies the integral constraint that the total number of radio sources must equal the total number of QSOs, and (3) best fits the observed flux-density distribution of faint sources; it is

$$n(S) = 0.11 S^{-1.8} \text{ Jy}^{-1} \text{ sr}^{-1}, S > S_{\text{min}} \quad (22)$$

and $n(S) = 0$ below $S_{\text{min}} = 0.018$ mJy. Of course, there is no reason to expect a break in the count slope to occur at the NVSS catalog limit, 2.4 mJy. At the midpoint of the QSO redshift range, $z = 2.15$, that break corresponds to a spectral luminosity $[\log L (\text{W Hz}^{-1})] \approx 25.8$, which is higher than the spectral luminosities of even the strongest starbursts.

Any more realistic extrapolation with a continuous count and count slope at 2.4 mJy must have a peak in $S^2 n(S)$ at lower flux densities to match the statistical data, as shown by an illustrative model that yields the dashed curve in Figure 8. Convolution of the model counts with the NVSS image noise distribution yields a good fit to the observed distribution of QSO peak flux densities; it is shown by the continuous curve in Figure 11). The median flux density of our high-redshift QSOs in this model is $\langle S \rangle \approx 0.05$ mJy, so the median 1.4 GHz spectral luminosity in the source frame (calculated assuming a median spectral index $\alpha = -0.7$) is $\log[(L_\nu(\text{W Hz}^{-1}))] \approx 24.1$ at $z = 2.15$. This is a factor of four higher than the 1.4 GHz spectral luminosity of Arp 220, and it might come from an AGN or a starburst. If it originates in a starburst obeying the FIR/radio correlation, an ultraluminous $[(L/L_\odot) \sim 4 \times 10^{12}]$ but not hyperluminous $[(L/L_\odot) > 10^{13}]$ starburst is required.

4. IS QSO RADIO EMISSION BIMODAL?

The first published claim of a bimodal flux-density distribution (Strittmatter et al. 1980) features a strong-source peak too narrow to be consistent with relativistic beaming. The Strittmatter et al. (1980) flux-density distribution plot is reproduced in Figure 12. The narrow peak in the quantity $\Delta \log N / \Delta \log S$ (where N is the number of sources stronger than S and $\Delta \log S = 0.2$ is the logarithmic width of each flux-density bin near $\log[S(\text{mJy})] = 3$ is an apparently significant factor of dex(2) ~ 100 higher than the long tail of fainter sources. We have inserted the actual numbers of radio sources contributing to each logarithmic flux-density bin into Figure 12. The peak is produced by only two sources, as N goes from 1 to 3, so $\Delta \log N = \log(3) - \log(1) \approx 0.48$ and $\Delta \log N / \Delta \log S \approx 0.48/0.2 \approx 2.4$ as plotted. However, the quantity $\Delta \log N / \Delta \log S$ is not the usual logarithmic differential source count or flux-density distribution $\log \Delta N / \Delta \log S$. The thin curve shows the distribution of $\Delta \log N / \Delta \log S$ that would result from the same total number of radio sources (ten) having a constant $\log \Delta N / \Delta \log S$ in the plotted flux-density range. Thus there is no significant peak in the nearly constant logarithmic differential flux-density distribution of these QSOs, which is consistent with our Equation 21.

Miller et al. (1990) made sensitive 5 GHz observations of 105 bright QSOs with $1.8 < z < 2.5$ selected by their emission lines. They found nine with $\log[L(\text{W Hz}^{-1})] > 26$ but none with $25 < \log[L(\text{W Hz}^{-1})] < 26$. All nine detections have $S > 20$ mJy, far above their $3\sigma \sim 0.6$ mJy detection limit. This is evidence for bimodal flux-density and luminosity distributions, but at what statistical significance? The nine detections have flux densities 21, 28, 28, 51, 76, 98, 105, 111, and 136 mJy. The likelihood of no weaker detections above 0.6 mJy depends on how the flux densities are binned. The bin limits should not be chosen *a posteriori* to minimize this probability. In bins of width dex(1) starting at the detection limit, there are $N = 0$ detections with $0.6 < S(\text{mJy}) < 6$, $N = 4$ detections with $6 < S(\text{mJy}) < 60$, and $N = 5$ detections with $60 < S(\text{mJy}) < 600$. If the flux-density distribution of $1.8 < z < 2.5$ QSOs is flat in logarithmic bins (as in Equation 21), there should be equal numbers in each bin. The average number of detections per bin is $\langle N \rangle = 3$, so

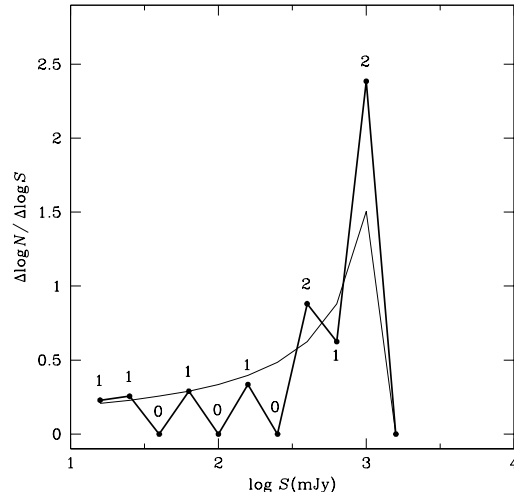


Figure 12. The differential flux-density distributions of QSOs as plotted by Strittmatter et al. (1980) with numbers of QSOs per bin added. The Poisson probability of no detections in the faintest bin is $P_P(0, 3) = \exp(-3) \approx 0.05$. Thus the lack of detections fainter than 6 mJy in this small sample may just be the result of bad luck, which we did not encounter in our much larger high-redshift QSO sample.

We prefer to study evolving QSO luminosity functions, which are intrinsic properties of QSOs, rather than flux-density distributions or luminosity distributions, which depend on observational parameters. We found that the luminosity functions $\rho_m(L)$ of radio sources so powerful that they must be produced by AGN are smooth and nearly flat power laws with no peaks or other features. There are “bumps” in the radio luminosity functions of QSOs, but they appear only at such low radio luminosities that the resulting radio flux densities are well below 1 mJy. The “bump” luminosities are consistent with significant starburst contributions (recall Figure 6): $\log[L(\text{W Hz}^{-1})] \sim 22.7$ for our moderate-luminosity QSOs at low ($0.2 < z < 0.45$) redshifts and $\log[L(\text{W Hz}^{-1})] \sim 24.1$, corresponding to an $(L/L_\odot) \sim 4 \times 10^{12}$ ultraluminous starburst, for the most luminous QSOs at higher redshifts, $1.8 < z < 2.5$.

5. THE AGN AND HOST GALAXY COMPONENTS OF QSO RADIO EMISSION

The radio emission from a QSO is the sum of contributions from its AGN and from star formation in its host galaxy. If the luminosities of the two contributions are nearly independent of each other at every redshift, the spectral luminosity function of QSOs will be the convolution of the AGN and starburst spectral luminosity functions.

5.1. Low-redshift QSOs

The AGN-powered portion of the luminosity function in the redshift range $0.2 < z < 0.45$ (Figure 4) was estimated from 163 NVSS detections of luminous sources. There are only 37 NVSS detections in the narrow redshift range $0.2 < z < 0.3$, too few for statistical accuracy, so we estimated the $0.2 < z < 0.3$ AGN luminosity function from the evolving AGN luminosity function in the redshift range $0.2 < z < 0.45$.

The luminosity function in the range $0.2 < z < 0.3$ is lower than the $0.2 < z < 0.45$ luminosity function by $\Delta \log \rho = -0.20$ (Sec. 2.3). This estimate is shown by the data points with error bars in Figure 6. For comparison, the 1.4 GHz local ($z \lesssim 0.05$) luminosity functions of galaxies (Condon, Cotton, & Broderick 2002) whose radio emission is dominated either by AGNs (continuous green curve) or by star formation (continuous red curve) are also shown. The radio luminosity function produced by AGNs in local galaxies is flatter and extends to higher radio luminosities than the luminosity function of star-forming galaxies, so local AGN-powered radio sources are more common above $\log[L_{1.4 \text{ GHz}}(\text{W Hz}^{-1})] = 23$ and star-forming galaxies have higher space densities than AGNs at lower luminosities. The luminosity $\log[L_{1.4 \text{ GHz}}(\text{W Hz}^{-1})] \approx 22$ of the galaxy M82 is typical for a nearby radio-selected star-forming galaxy.

Even allowing for starburst luminosity evolution, it is likely that the radio emission of low redshift ($0.2 < z < 0.45$) QSOs stronger than $\log[L_{1.4 \text{ GHz}}(\text{W Hz}^{-1})] = 24$ is dominated by AGNs. To estimate the luminosity function that would result if all QSO radio emission were powered by only by AGNs, even at lower luminosities, we made the smooth power-law extrapolation (dashed green line in Figure 6) of the observed QSO luminosity function to lower luminosities. This extrapolation must be truncated below $\log[L_{1.4 \text{ GHz}}(\text{W Hz}^{-1})] \sim 20$, as suggested by the dotted green curve in Figure 6, to keep the number of radio sources from exceeding the total number of low-redshift QSOs (1313). The details of the AGN luminosity function below $\log[L_{1.4 \text{ GHz}}(\text{W Hz}^{-1})] \approx 22$ are not well known but don't matter because any luminosity function in this range always predicts that most of the low-redshift QSOs powered by entirely by AGN would be too radio quiet (< 0.02 mJy) to be statistically detectable by the NVSS. The dashed curve in Figure 5 shows the AGN-only flux-density distribution predicted by this model for the $0.2 < z < 0.3$ QSOs. The distribution peak flux density $\langle S_p \rangle \approx 0.05$ mJy beam $^{-1}$ is much lower than the observed $\langle S_p \rangle \approx 0.33$ mJy beam $^{-1}$. The AGN-only distribution is distinguishable from the blank-sky distribution (dotted curve) only because its height has been depressed by the loss of QSOs in the long tail of strong sources above 2.5 mJy beam $^{-1}$, which are off scale on this plot. The failure of the dashed curve to fit the data suggests that most of the low-redshift QSOs are not in “red and dead” elliptical galaxies with little or no ongoing star formation.

Any QSO luminosity function that is consistent with both the NVSS direct detections of sources stronger than 2.4 mJy and the distribution of peak flux densities in Figure 5 must rise sharply just below $\log[L_\nu(\text{W Hz}^{-1})] = 24$ and fall fairly quickly at lower luminosities lest it imply more than 1313 SDSS QSOs with $0.2 < z < 0.45$. Kimball et al. (2011) proposed that radio emission from the star-forming host galaxies is the cause of that rise. The peak of the the QSO host-galaxy radio luminosity function (dashed red curve in Figure 6) is at $\log[L_\nu(\text{W Hz}^{-1})] \approx 22.7$. If the faint radio sources are dominated by emission from the star-forming host galaxies, their radio spectral indices between 1.4 GHz

and 6 GHz should be $\alpha \approx -0.7$, which is the observed value (Kimball et al. 2011).

As it must, the radio luminosity function of the low-redshift QSO host galaxies lies below the radio luminosity function of *all* nearby galaxies powered primarily by star formation, but it is not much lower at the highest radio luminosities because many low-redshift QSOs seem to have high star-formation rates. The radio luminosity function of QSO host galaxies must fall rapidly below $\log[L_{1.4 \text{ GHz}}(\text{W Hz}^{-1})] \sim 20$ to satisfy the constraint that its integral not exceed the total number of SDSS QSOs in $0.2 < z < 0.3$. In this respect, it differs from the radio luminosity function of all nearby star-forming galaxies (red curve in Figure 6), which rises slowly but monotonically even at very low luminosities. This difference is not surprising: most of the faintest nearby radio sources lie in low-mass galaxies with low star-formation rates (Condon, Cotton, & Broderick 2002), while QSOs are found only in massive galaxies. The real surprise to radio astronomers accustomed to comparing QSOs with radio galaxies is that massive elliptical galaxies with low star-formation rates are so rare in our low-redshift QSO sample.

5.2. High-redshift QSOs

The high statistical detection rate of $1.8 < z < 2.5$ QSOs reported in Sec. 3.1 shows that most of these very luminous (median $\langle M_i \rangle \approx -27.5$) high-redshift QSOs contain radio sources with median spectral luminosity $\log[L_{1.4 \text{ GHz}}(\text{W Hz}^{-1})] \approx 24.1$. This high detection rate is not consistent with a power-law extrapolation from higher radio luminosities of the AGN luminosity function; there must also be a “bump” in the QSO radio luminosity function at high redshifts. As illustrated in Figure 8, the bump must lie in a fairly narrow flux-density range $-5 < \log[S(\text{Jy})] < -3$ to be consistent with the distribution of NVSS peak flux densities (Figure 11). Such a bump is consistent with, but does not by itself require, radio emission from ultraluminous [$(L/L_\odot) \sim 4 \times 10^{12}$] starbursts in the host galaxies of the most luminous QSOs. Should we expect that most luminous, high-redshift QSOs contain ultraluminous starbursts?

The presence of a luminous QSO implies a high rate of radiatively efficient accretion onto a supermassive black hole. During “quasar mode” or “cold mode” accretion (Croton et al. 2006), cold gas is rapidly fed via an accretion disk to the black hole. The reservoir of cold gas that feeds the AGN may also produce a burst of star formation, as suggested by recent observations starbursts in the host galaxies of high-luminosity ($L_x > 10^{37}$ W) X-ray QSOs with $z \gtrsim 2$ (Rovilos et al. 2012) and of infrared emission from cold dust in the host galaxies of the fairly luminous ($\langle M_i \rangle \approx -25$) QSOs found in the Herschel ATLAS survey (Bonfield et al. 2011). Bonfield et al. (2011) associated the total ($8 \mu < \lambda < 1000 \mu$) infrared luminosity L_{IR} with the star-formation luminosity and found it is related to the QSO luminosity L_{QSO} via

$$L_{\text{IR}} \propto L_{\text{QSO}}^\theta (1+z)^\zeta, \quad (23)$$

where $\theta = 0.22 \pm 0.08$ and $\zeta = 1.6 \pm 1$. Using the FIR/radio correlation (Condon 1992) and the median 1.4 GHz spectral luminosity, we estimate the median

starburst luminosity $\log(L_{\text{IR}}/L_{\odot}) \approx 11.2$ for our low-redshift QSOs at typical redshift $z \approx 0.35$. The median absolute magnitudes of the low- and high-redshift QSOs are $M_i = -23.38 \pm 0.03$ and $M_i = -27.48 \pm 0.01$, for a QSO luminosity ratio ≈ 44 . Inserting these values into Equation 23 indicates that our high-redshift ($z \approx 2.15$) QSOs should have a median starburst luminosity $\log(L/L_{\odot}) = 12.2 \pm 0.4$ and a median radio spectral luminosity $\log[L_{1.4 \text{ GHz}}(\text{W Hz}^{-1})] = 23.7 \pm 0.4$, only one sigma below our observed median $\log[L_{1.4 \text{ GHz}}(\text{W Hz}^{-1})] = 24.1$ for SDSS QSOs in the redshift range $1.8 < z < 2.5$.

6. SUMMARY

We investigated the 1.4 GHz radio emission from large optically selected samples of SDSS DR7 QSOs in two redshift ranges: $0.2 < z < 0.45$ and $1.8 < z < 2.5$. As expected, only about 10% of the QSOs are sufficiently radio loud to be detected above the $S = 2.4$ mJy NVSS catalog limit. Such sources are so luminous that the bulk of their radio emission must be powered by AGNs. The 1.4 GHz luminosity functions of AGN-powered sources both samples (Figures 4 and 10) are flat power laws, so flat that the number of sources per decade of flux density or luminosity is nearly constant. These luminosity functions show no features or signs of bimodality that might indicate two or more distinct QSO types among the $\sim 10\%$ of QSOs that are in the NVSS catalog.

Extrapolating the flat luminosity functions to lower luminosities predicts that most of the undetected QSOs should be extremely faint radio sources. However, the distributions of peak flux densities at QSO positions on the NVSS images reveal that most QSOs are moderately luminous radio sources, so there must be peaks or “bumps” in their 1.4 GHz luminosity functions in both redshift ranges. QSOs with $0.2 < z < 0.3$ have a median peak flux density $S_p \approx 0.3 \text{ mJy beam}^{-1}$ (Figure 5) and median spectral luminosity $\log[L_{1.4 \text{ GHz}}(\text{W Hz}^{-1})] \approx 22.7$; QSOs in the redshift range $1.8 < z < 2.5$ have a median peak flux density $S_p \approx 0.05 \text{ mJy beam}^{-1}$ (Figure 11) and median spectral luminosity $\log[L_{1.4 \text{ GHz}}(\text{W Hz}^{-1})] \approx 24.1$. The reality of the statistical detections in the narrow redshift range $0.2 < z < 0.3$ was confirmed by individual detections of nearly all of these QSOs by the VLA at 6 GHz (Kimball et al. 2011), and the median spectral index of these sources is $\langle \alpha \rangle \approx -0.7$, typical of optically thin synchrotron emission from either AGNs or star-forming galaxies.

We suggest that the faint radio sources found in most bright optically selected QSOs are primarily powered by star formation. The median radio luminosities correspond to star-formation rates $\dot{M} \sim 20M_{\odot} \text{ yr}^{-1}$ and $\dot{M} \sim 500M_{\odot} \text{ yr}^{-1}$ for the moderately luminous ($\langle M_i \rangle \approx -23.4$) QSOs with $0.2 < z < 0.45$ and the extremely luminous ($\langle M_i \rangle \approx -27.5$) QSOs with $1.8 < z < 2.5$, respectively. The total infrared luminosities of such starbursts can be estimated from the FIR/radio correlation. They are $\log(L_{\text{IR}}/L_{\odot}) \approx 11.2$ for the $0.2 < z < 0.45$ QSOs and $\log(L_{\text{IR}}/L_{\odot}) \approx 12.6$ for the $1.8 < z < 2.5$ QSOs. Such powerful starbursts may be fueled by the same cold gas reservoirs that flow into the central supermassive black holes that power the QSOs themselves. Our starburst

interpretation of the low-luminosity QSO radio emission is supported by (1) far-infrared detections of cold dust in QSO host galaxies (Bonfield et al. 2011), and (2) agreement of our radio results with their empirical scaling of L_{IR} with QSO luminosity and redshift.

With cm-wavelength radio data alone, it is difficult to test our hypothesis that star formation in the host galaxies of most QSOs powers the faint radio sources that make the “bumps” in our otherwise flat radio luminosity functions and source counts. One way would be to show that the faint radio sources in QSOs follow the tight FIR/radio correlation obeyed by nearly all starburst galaxies. However, it is necessary to distinguish the FIR emission from a large mass of cool dust heated by stars from the mid-infrared (MIR) emission from a small mass of warmer dust heated by an AGN (Morić et al. 2010), so it is preferable that the dust flux density be measured in the Rayleigh-Jeans tail at submillimeter wavelengths, by ALMA for example. Alternatively, ALMA submillimeter spectroscopy of molecular and ionic lines sensitive to X-ray dominated regions might reveal deeply buried AGNs (Rangwala et al. 2011).

REFERENCES

- Baloković, M., Smolčić, V., Ivezić, Z., et al. 2012, *ApJ*, in press (arXiv:1209.1099B)
- Barthel, P. D. 2006, *A&A*, 458, 1007
- Barvainis, R. 1990, *ApJ*, 353, 419
- Barvainis, R., Lehar, J., Birkinshaw, M., Falcke, H., & Blundell, K. M. 2005, *ApJ*, 618, 108
- Becker, R. H., White, R. L., & Helfand, D. J. 1995, *ApJ*, 450, 559
- Blundell, K. M., & Beasley, A. J. 1998, *MNRAS*, 299, 165
- Blundell, K. M., & Kuncic, Z. 2007, *ApJ*, 668, L103
- Bonfield, D. G., Jarvis, M. J., Hardcastle, M. J. et al. 2011, *MNRAS*, 416, 13
- Boyce, P. J., Disney, M. J., Blades, J. C., et al. 1998, *MNRAS*, 298, 121
- Condon, J. J. 1992, *ARA&A*, 30, 575
- Condon, J. J., Cotton, W. D., & Broderick, J. J. 2002, *AJ*, 124, 675
- Condon, J. J., Huang, Z.-P., Yin, Q. F., & Thuan, T. X. T. 1991, *ApJ*, 378, 65
- Condon, J. J., & Mitchell, K. J. 1984, *AJ*, 89, 610
- Condon, J. J., Cotton, W. D., Greisen, E. W., et al. 1998, *AJ*, 115, 1693 (NVSS)
- Condon, J. J., Cotton, W. D., Yin, Q. F., et al. 2003, *AJ*, 125, 2411
- Cotton, W. D., Wittels, J. J., Shapiro, I. I. et al. 1980, *ApJ*, 238, L123
- Crawford, D. F., Jauncey, D. L., & Murdoch, H. S. 1970, *ApJ*, 162, 405
- Croton, D. J., Springel, V., White, S. D. M. et al. 2006, *MNRAS*, 365, 11
- de Vries, W. H., Hodge, J. A., Becker, R. H., White, R. L., & Helfand, D. J. 2007, *AJ*, 134, 457
- Dunlop, J. S., McLure, R. J., Kucula, M. J., et al. 2003, *MNRAS*, 340, 1095
- Falcke, H., Patnaik, A. R., & Sherwood, W. 1996, *ApJ*, 473, L13
- Greenstein, J. L., & Matthews, T. A. 1963, *Nature*, 197, 1041
- Hazard, C., Mackey, M. B., & Shimmins, A. J. 1963, *Nature*, 197, 1037
- Hoyle, F., & Burbidge, G. R. 1966, *ApJ*, 144, 534
- Ivezić, Z., Menou, K., Knapp, G. R., et al. 2002, *AJ*, 124, 2364
- Kamionkowski, M., & Loeb, A. 1997, *Phys.Rev.D*, 56, 4511
- Katgert, P., Katgert-Merkelijn, J. K., Le Poole, R. S., & van der Laan, H. 1973, *A&A*, 23, 171
- Kellermann, K. I., & Pauliny-Toth, I. I. K. 1966, *Nature*, 212, 781
- Kellermann, K. I., Sramek, R., Schmidt, M., Shaffer, D. B., & Green, R. 1989, *AJ*, 98, 1195
- Kellermann, K. I., Sramek, R. A., Schmidt, M., Green, R. F., & Shaffer, D. B. 1994, *AJ*, 108, 1163
- Kimball, A. E., Kellermann, K. I., Condon, J. J., Ivezić, Z., & Perley, R. A. 2011, *ApJ*, 739, L29
- Mahony, E., Sadler, E. M., Croom, S. M. et al. 2012, *ApJ*, 754, 12
- Matthews, T. A., & Sandage, A. R. 1963, *ApJ*, 138, 30
- Miller, L., Peacock, J. A., & Mead, A. R. G. 1990, *MNRAS*, 24, 207
- Miller, P., Rawlings, S., & Saunders, R. 1993, *MNRAS*, 263, 425
- Mitchell, K. J., & Condon, J. J. 1985, *AJ*, 90, 1957
- Morić, L., Smolčić, V., Kimball, A., et al. 2010, *ApJ*, 724, 779
- Mundell, C. G., Ferruit, P., & Pedlar, A. 2001, *ApJ*, 560, 168
- Peacock, J. A., Miller, L., & Longair, M. S. 1986, *MNRAS*, 218, 265
- Rangwala, N., Maloney, P. R., Glenn, J., et al. 2011, *ApJ*, 743:94
- Rovilos, E., Comastri, A., Gilli, R. et al. 2012, *A&A*, in press (arXiv:1207.7129)
- Sandage, A. 1965, *ApJ*, 141, 1560
- Scheuer, P. A. G., & Readhead, A. C. S. 1979, *Nature*, 277, 182
- Schmidt, M. 1963, *Nature*, 197, 1040
- Schmidt, M. 1970, *ApJ*, 162, 371
- Schmidt, M., & Green, R. F. 1983, *ApJ*, 269, 352
- Schneider, D. P., Richards, G. T., Hall, P. B. et al. 2010, *AJ*, 139, 2360
- Sopp, H. M., & Alexander, P. 1991, *MNRAS*, 251, 14P
- Steenbrugge, K. C., Jolley, E. J. D., Kuncic, Z., & Blundell, K. M. 2011, *MNRAS*, 413, 1735
- Strittmatter, P. A., Hill, P., Pauliny-Toth, I. I. K., Steppe, H., & Witzel, A. 1980, *A&A*, 88, L12
- Ulvestad, J. S., Antonucci, R. R. J., & Barvainis, R. 2005, *ApJ*, 621, 123
- Walsh, D. E. P., Knapp, G. R., Wrobel, J. M., & Kim, D.-W. 1989, *ApJ*, 337, 209
- White, R. L., Becker, R. H., Helfand, D. J., & Gregg, M. D. 1997, *ApJ*, 475, 479
- White, R. L., Helfand, D. J., Becker, R. H., Glikman, E., & de Vries, W. 2007, *ApJ*, 654, 99

Table 1
NVSS-detected QSOs, $0.2 < z < 0.45$

RA (J2000)	DEC	Redshift z	M_i	S (mJy)	$\log L_{1.4}$ (W Hz $^{-1}$)
07 54 03.61	+48 14 28.1	0.2755	-23.478	7.3	24.19
08 06 44.43	+48 41 49.2	0.3701	-23.769	901.7	26.57
08 20 15.61	+59 42 28.4	0.3676	-25.461	5.6	24.36
08 33 53.88	+42 24 01.9	0.2491	-23.903	248.6	25.62
08 36 58.91	+44 26 02.3	0.2544	-24.999	6.6	24.07
08 43 10.79	+39 53 45.1	0.4036	-23.765	2.6	24.12
08 43 47.85	+20 37 52.5	0.2273	-23.034	59.7	24.92
08 49 40.01	+09 49 21.1	0.3656	-23.425	587.2	26.37
08 50 39.96	+54 37 53.3	0.3673	-23.076	166.5	25.83
08 55 16.21	+56 16 56.8	0.4422	-23.759	5.3	24.52
08 56 32.99	+59 57 46.9	0.2830	-23.858	239.4	25.73

Note. — Table 1 is published in its entirety in the electronic edition of the *Astrophysical Journal*. A portion is shown here for guidance regarding its form and content.

Table 2
NVSS “snapshot bias”

FLS flux density (μ Jy)	Number of sources	NVSS bias (μ Jy beam $^{-1}$)
115–160	937	-17 \pm 15
160–230	821	+7 \pm 16
230–460	771	+29 \pm 17
115–460	2550	+3 \pm 9

Table 3
NVSS-detected QSOs, $1.8 < z < 2.5$

RA (J2000)	DEC	Redshift z	M_i	S (mJy)	$\log L_{1.4}$ (W Hz $^{-1}$)
08 06 20.47	+50 41 24.4	2.4565	-28.38	16.9	26.75
08 11 41.98	+51 57 10.9	2.1763	-27.65	5.1	26.12
08 21 53.82	+50 31 20.4	2.1326	-27.93	58.5	27.16
08 27 54.25	+33 36 04.2	1.8056	-27.04	31.5	26.72
08 33 50.61	+38 39 22.8	2.0143	-27.53	2.7	25.76
08 34 00.05	+43 01 48.1	2.3916	-27.39	19.0	26.78
08 37 22.41	+58 25 01.8	2.1010	-27.89	690.4	28.21
08 45 06.24	+42 57 18.4	2.0945	-27.38	224.0	27.72
08 45 47.19	+13 28 58.1	1.8834	-28.40	413.4	27.88
08 50 51.80	+15 22 15.0	2.0183	-27.85	520.2	28.05

Note. — Table 3 is published in its entirety in the electronic edition of the *Astrophysical Journal*. A portion is shown here for guidance regarding its form and content.